Fluorescence Microscopy: A Concise Guide to Current Imaging Methods

Christian A. Combs[1] and Hari Shroff[2]

[1]NHLBI Light Microscopy Facility, National Institutes of Health, Bethesda, Maryland
[2]NIBIB Section on High Resolution Optical Imaging, National Institutes of Health, Bethesda, Maryland

The field of fluorescence microscopy is rapidly growing and offers ever more imaging capabilities for biologists. Over the past decade, many new technologies and techniques have been developed that allow for combinations of deeper, faster, and higher resolution imaging. These have included the commercialization of many super-resolution and light sheet fluorescence microscopy techniques. For the non-expert, it can be difficult to match the best imaging techniques to biological questions. Picking the most appropriate imaging modality requires a basic understanding of the underlying physics governing each of them, as well as information comparing potentially competing imaging properties in the context of the sample to be imaged. To address these issues, we provide here concise descriptions of a wide range of commercially available imaging techniques from wide-field to super-resolution microscopy, and provide a tabular guide to aid in comparisons among them. In this manner we provide a concise guide to understanding and matching the correct imaging modality to meet research needs. © 2017 by John Wiley & Sons, Inc.

Keywords: confocal • light-sheet • review • super-resolution • two-photon

How to cite this article:
Combs, C. A., & Shroff, H. (2017). Fluorescence microscopy: A concise guide to current imaging methods. *Current Protocols in Neuroscience*, *79*, 2.1.1–2.1.25.
doi: 10.1002/cpns.29

INTRODUCTION

Fluorescence microscopy (FM) is a powerful tool for cell and molecular biologists. It provides a window into the physiology of living cells at sub-cellular resolution allowing for direct visualization of the inner workings of physiological processes. Recently there has been a revolution in FM (Cox & Jones, 2013; Han, Li, Fan, & Jiang, 2013; Toomre & Bewersdorf, 2010). The resolution limit for light microscopy (the diffraction limit described by Ernst Abbe, ~200 nm) has been shattered by many super-resolution techniques, and the capacity for 3-D imaging over time ("4D" imaging) has been greatly improved with Light Sheet Microscopy. Along with these advances, the utility of standard techniques, such as confocal microscopy and two-photon fluorescence microscopy (TPFM), have been improved. Many of the new advanced techniques are now being commercialized, opening their use to ever more biologists. This revolution in techniques is also supported by the many improved fluorescent probes and proteins that are now available (for reviews, see Shaner, Steinbach, & Tsien, 2005; Uno et al., 2015; Ni, Zhuo, So, & Yu, 2016b). This expansion in capabilities explains why thousands of papers utilizing these imaging methods are published each year. For the biologist inexperienced in light microscopy, however, matching the best technique to a biological experiment can be difficult. Optimal use of fluorescence microscopy requires a basic understanding of the strengths and weaknesses of the various techniques, as well as an understanding of the fundamental trade-offs associated with fluorescent light collection.

In a very simple form, the ideal light microscopy experiment can be viewed as optimizing the competing properties and trade-offs of image resolution (in the *XY* or lateral

Current Protocols in Neuroscience 2.1.1–2.1.25, April 2017
Published online April 2017 in Wiley Online Library (wileyonlinelibrary.com).
doi: 10.1002/cpns.29

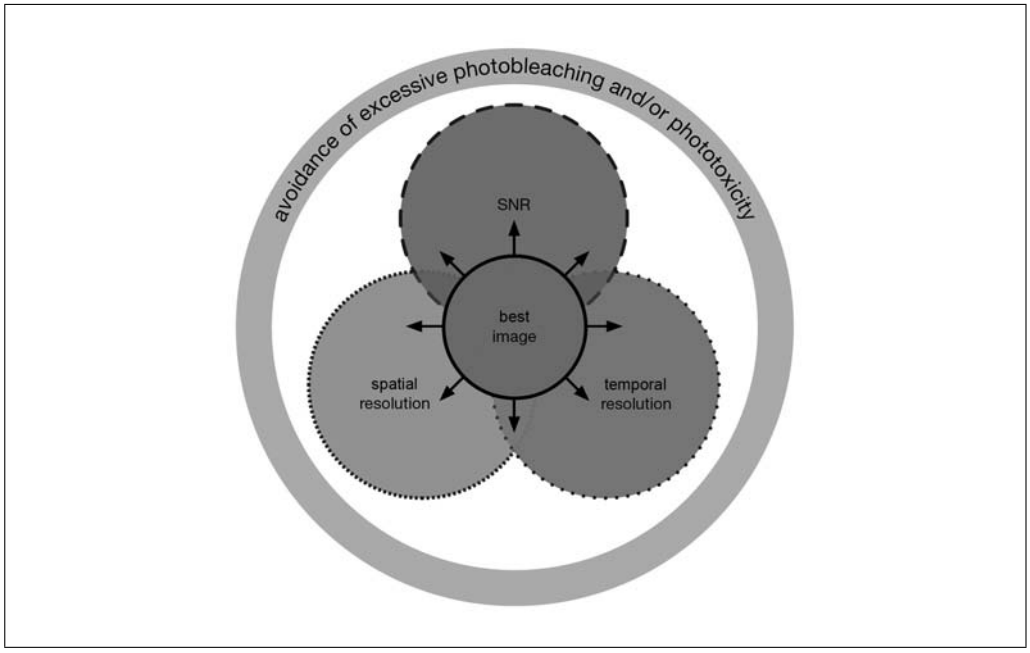

Figure 2.1.1 Tradeoffs in an imaging experiment. The best image is one that can balance these factors to obtain the necessary information while avoiding photobleaching or phototoxic effects. Table 2.1.2 outlines how these factors differ between the various commercialized microscopy techniques discussed in this work. SNR = signal-to-noise ratio.

direction as well as the *Z* or axial dimension), imaging speed (and/or acquisition time), and the amount of signal collected from the fluorescing sample (Fig. 2.1.1). In addition, this optimization problem is constrained by the limits imposed by photobleaching and/or phototoxicity, especially in live samples. In many experiments, light levels at the diffraction limited spot (focused by the objective) can be very high. This can lead to destruction of the fluorophore and unwanted biological consequences leading to cell death or changes in the physiology of the cells or tissue being illuminated. Given such constraints, these variables are difficult to balance and require careful attention to detailed and systematic (and often sample-specific) empirical testing. On top of these basic variables, other secondary variables also become important, including the cost of the necessary equipment and the difficulty of the technique.

In this review, knowledge of the fundamentals of fluorescence will be assumed. The objective is to provide non-experts with a concise description and guide to selecting among the commercially available microscopy techniques. The techniques discussed encompass the most basic (such as wide-field fluorescence microscopy) to cutting edge super-resolution techniques. Emphasis is placed on explaining the strengths and weaknesses of these techniques in terms of balancing the variables discussed in Figure 2.1.1. The field of fluorescence microscopy is acronym rich. Table 2.1.1 provides an abbreviation guide to aid reading this manuscript. Table 2.1.2 summarizes this discussion and should serve as a quick guide for choosing the appropriate imaging modality from among the techniques discussed.

WIDE-FIELD FLUORESCENCE MICROSCOPY (WFFM) TECHNIQUES

In the most basic form, wide-field fluorescence microscopy (WFFM), also referred to as epi-fluorescence microscopy, elicits fluorescence from the sample using a light source, a microscope, and excitation and emission filters. The resulting emitted light, of longer wavelength than the excitation, is collected by the objective lens and observed through the microscope eyepieces or by a camera followed by computer digitization (for reviews, see Coling & Kachar, 2001; Inoue & Spring, 1997; Lichtman & Conchello, 2005). Although the basics of WFFM have not changed, there have been recent improvements that allow for better imaging. These include better cameras, objectives, optical filters, and computers. Perhaps the biggest advances are improvements in the cameras used for imaging. Modern cameras now allow for very large formats (several megapixels), high sensitivity (>50% quantum efficiency) and dynamic range, lower noise

Table 2.1.1 List of the Meanings of Selected Abbreviations in the Text

CW	Continuous wave
DFM	Deconvolution fluorescence microscopy
EMCCD	Electron multiplying charge-coupled device camera
FM	Fluorescence microscopy
FRAP	Fluorescence recovery after photobleaching
FRET	Fluorescence resonance energy transfer
FWHW	Full-width half maximum
GFP	Green fluorescent protein
GSDIM	Ground state depletion microscopy
IR	Infrared
iSIM	Instant structured illumination microscopy
LED	Light-emitting diode
LSCM	Laser scanning fluorescence microscopy
LSFM	Light sheet fluorescence microscopy
mW	Milliwatts
μW	Microwatts
NA	Numerical aperture
OPO	Optical parametric oscillator
PAINT	Point accumulation for imaging in nanoscale topography
PALM	Photoactivated localization microscopy
PMT	Photo-multiplier tube
PSF	Point spread function
ROI	Region of interest
sCMOS	Scientific complimentary metal-oxide-semiconductor camera
SHG	Second-harmonic generation
SIM	Structured illumination microscopy
SLM	Structured light microscopy
SMLM	Single molecule localization microscopy
SNR	Signal-to-noise ratio
SPIM	Single plane illumination microscopy
STED	Stimulated emission depletion microscopy
STORM	Stochastic optical reconstruction microscopy
TIRF	Total internal reflection fluorescence microscopy
TPFM	Two-photon fluorescence microscopy
WFFM	Wide-field fluorescence microscopy
UV	Ultraviolet

characteristics (~1 electron read noise), and faster frame rates (hundreds to thousands of frames per second) than their predecessors of just a few years ago. These advances allow for faster imaging and better contrast at low signal levels (when the excitation light is deliberately minimized to prevent photobleaching or phototoxicity), while preserving the potential for diffraction-limited resolution over large fields of view. Modern camera types include scientific complementary metal oxide semiconductor (sCMOS) and electron multiplied charge coupled device (EMCCD) cameras. sCMOS cameras, with their large chip

Table 2.1.2 Comparison of Selected Characteristics of Commercially Available Microscope Techniques Discussed in This Unit (Black Boxes are Best in Category, Gray are Worst)

Technique	Resolution *XY*	Resolution *Z*	Resolution temporal	Imaging depth	Usability	Cost[a]	SNR[b]	Photobleaching/ phototoxicity
Wide-field (WF)	Diffraction limited (≈200 nm)	Poor (usually worse than 1 μm)	Best (msec/ frame, signal limited)	Worst	Simple	$	High	Best (usually μWatts distributed over large imaging field)
Total Internal Reflection (TIRF)	Diffraction limited but low background	Best but only first 200-300 nm	Good (msec/frame, signal limited)	<300 nm	Good	$$	High	Better
Laser-Scanning Confocal (LSCM)	Diffraction limited to nearly 2× diffraction limit (Airy Scan)	Good (better than 700 nm)	Varies with scanner type (typically 1-30 f.p.s)	Better (less than 100 μm)	Complex but most versatile	$2-$7	Moderate	Can be bad (μWatts of power focused to spot)
Multi-point/ slit confocal	Diffraction limited	Good (slightly worse than LSCM)	Good (msec/ frame, signal limited)	Typically <50μm	Better	$2-$4	Moderate	Better (usually lower excitation flux density than LSCM)
Two-Photon Fluorescence Microscopy (TPFM)	Diffraction limited	Good (slightly less than LSCM)	Varies with scanner type (typically 1-30 f.p.s)	Best (hundreds of μms)	Complex	$3-$7 with 1 pulsed laser	Moderate	Can be bad (μWatts power focused to spot but only eliciting fluorescence from the focal plane)
Structured Light Microscopy (SIM)	Diffraction limited	Good – usually worse than LSCM	Typically 1-10 fps	Typically <30 μm	Simple	$1.5	Moderate	Good (varies with number of images needed)
Super-resolution SR-SIM	Super-Resolution to at least 2× diffraction limit with deconvolution	To 2× diffraction limit with de-convolution	Good (can be msec/frame with iSIM, signal limited)	Typically <10 μm, iSIM < 50 μm	Better (if decon-volved)	$4-$9	Moderate	Typically good
Stimulated Emission Depletion (STED)	Super-resolution (<70 nm	Same as LSCM or < 100 nm with axial phase plate	Varies with scanner type (typically 1-30 f.p.s)	Typically <50 μm	Complex	$6-$10	Low	Worst (second beam with many μWatts of power)
Single Molecule (SMLM)*c**	Best Super-resolution (<30 nm)	Can be ~100 nm or less	Worst Requires thousands of images	Typically less than a few μm or less than 200 nm	Complex and requires post-processing	$3-$4	Low (noisy if marker density too low)	Varies with technique, can be harsh, typically requires thousands of images

continued

Table 2.1.2 Comparison of Selected Characteristics of Commercially Available Microscope Techniques Discussed in This Unit (Black Boxes are Best in Category, Gray are Worst), *continued*

Technique	Resolution *XY*	Resolution *Z*	Resolution temporal	Imaging depth	Usability	Cost[a]	SNR[b]	Photobleaching/ phototoxicity
Light Sheet Fluorescence Microscopy (LSFM)	Diffraction Limited but typically low-mid level NA lenses are used	Good depends on light sheet thickness and objective NA	Best for 3-D imaging	Best (hundreds of microns)	Better but requires calibration	$2-$6	High	Best for 3D (Z stack) or 4D (Z- stack over time) imaging
Lattice Light Sheet with SIM	Super-resolution to 2× diffraction limit with deconvolution	Super-resolution to 2× diffraction limit with de-convolution	Best for 3-D imaging	Typically <20 μm	Complex	$2-$6	Moderate	Best for 3D (Z stack) or 4D (Z stack over time) imaging

[a]A single $ refers to the cost of a state of the art widefield microscope. In today's dollars approximately $70-$100,000.
[b]SNR-Relative signal-to-noise ratio.
[c]SMLM-Single Molecule Localization Microscopy includes Ground State Depletion (GSD), Photoactivatable Localization Microscopy, and Stochastic Optical Reconstruction Microscopy (STORM)

sizes, small pixels (enabling higher resolution for a given field of view), and high temporal resolution, are best for most demanding applications. While sCMOS cameras may eventually outcompete EMCCD cameras in all applications, EMCCDs currently are still best for imaging at exceedingly low light levels (<10 photoelectrons/pixel).

In addition to cameras, wide-field microscopy has also been improved by better filters, dichroic mirrors, and objectives. Commercially available filters, for instance from Chroma (Rockinham, VT) or Semrock (Rochester, NY), have very high transmittance or reflection, and due to new sputter-coating technologies, do not degrade over time. In addition, these filters can have very sharp wavelength dependencies that enable excellent multi-color discrimination. In the past decade, all of the major microscope companies (such as Leica, Nikon, Olympus, and Zeiss) have also improved microscope objectives. These new objectives have very flat fields (which decrease objective-induced gradients in intensity across an image, or distortions at the edges of the field of view), long working distances with good resolving power, improved light transmission from the near UV to the infrared, and are increasingly available in varieties that match the refractive index of the sample being imaged.

The main advantages of basic WFFM are that it is the least expensive technique, it provides good XY (lateral) resolution (the ability to distinguish fine detail in a specimen in the lateral dimension), can provide very fast temporal resolution (particularly with the new sCMOS cameras), and in many cases uses the least amount of excitation (Table 2.1.2). XY resolution ($R_{x\,y}$) in wide-field microscopy is determined by the numerical aperture (NA) of the objective lens and the wavelength of the excitation light according to Ernst Abbe's diffraction limit expression:

$$R_{xy} \approx 0.61\lambda/NA$$

Equation 2.1.1

where λ is the wavelength of the emitted light and NA is the numerical aperture of the objective.

For a high NA objective (e.g., NA 1.4) lens, this limit is theoretically around 200 nm using blue light, although in practice optical aberrations limit wide-field resolution to >250 nm. The resolution of a given system in all dimensions can be estimated from the point spread function (PSF) that a microscope produces (although the PSF may vary across the field of view and with depth). The PSF is the 2-D or 3-D image resulting from a sub-resolution point-like object (typically in fluorescence microscopy this is measured using a fluorescent bead that is less than 0.2 μm in size, although smaller resolution targets must be used for PSF determination when doing super-resolution imaging) as imaged through an objective lens. Examples of PSFs are shown in Figures 2.1.10A and 2.1.10B.

All of the techniques listed in Table 2.1.2 are approximately limited to this type of XY resolution, except where super-resolution is indicated.

The main disadvantage of basic WFFM is that that all of the emitted light is integrated through the sample in the *Z* dimension (i.e., the axial dimension), i.e., there is no "optical sectioning" in the WFFM. Therefore, it is difficult to precisely assign the fluorescence to its correct axial coordinate, and the presence of out-of- focus light greatly reduces contrast in thick, densely labeled samples. For thin samples (<5 μm), or where axial discrimination is not critical this may not be a limiting factor. For thick samples, such as tissues or large live cells, where optical sectioning is critical or where out-of-focus light swamps details even in the *XY* plane, other techniques such as confocal or multi-photon microscopy may be more appropriate (see the following sections), although deconvolution microscopy and structured light microscopy (SLM) are alternative WFFM techniques that are commercially available and also improve axial resolution. Deconvolution techniques and SLM are discussed in their own sections in this review.

TOTAL INTERNAL REFLECTION FLUORESCENCE (TIRF) MICROSCOPY

TIRF microscopy can provide very good axial discrimination (*Z* direction, along the axis of illumination) (for review, see Toomre & Manstein, 2001) allowing for selective imaging of events (cellular membrane binding events, membrane dynamics, cell adhesion, etc.) very close to (within 100 nm of) the coverslip. Not only does this capability provide better axial resolution than most other techniques but it also can greatly reduce background light (thus increasing the signal to noise ratio) that would otherwise obscure fine details. The setup for TIRF microscopy is very simple and is similar to wide-field microscopy, except that it employs an oblique angle for the excitation light impinging on the sample. When the incidence angle is set to a critical angle relative to the coverslip, and the coverslip is of higher index than the imaging medium and sample, the excitation light is totally internally reflected (Fig. 2.1.2A). This generates an electromagnetic field at the interface, called an evanescent wave, which excites fluorophores in nearly the same manner as conventional excitation light. The key difference is that the evanescent wave propagates only a short distance above the coverslip (Fig. 2.1.2B). Therefore, only fluorescent molecules in close proximity (< 300 nm) to the coverslip are excited. Figure 2.1.2C and 2D show wide-field and TIRF images, respectively, of the fluorescence from EGFP-labeled myosin in drosophila embryo hemocytes. As can be seen in Figure 2.1.2D, only myosin molecules in portions of the cell near the coverslip are excited, thus selectively highlighting these regions of the sample.

The decay of the evanescent wave is exponential with the distance above the coverslip. This relationship can be expressed as:

$$I(z) = I(0)\, e^{-z/d}$$

Equation 2.1.2

where I(z) represents the intensity at a given distance (z) from the coverslip, I(0) is the intensity at the coverslip, and d is the penetration depth in microns. The penetration depth d decreases as the reflection angle of the incident beam (θ_C, shown in Figure 2.1.2) grows larger. This value is also dependent on the illumination wavelength and on the refractive index of the medium present at the interface. In a typical commercially available objective-based TIRF system, the reflection angle of the excitation light can be changed using a special illumination module attached to the epi-fluorescence port of a wide-field microscope. Turning the micrometer changes the position of the beam traveling in the periphery of the objective's back aperture, resulting in a change in the angle of the beam exiting the front element.

Another requirement for the typical objective-based TIRF system is that high numerical oil objectives (>1.4 NA) are required to generate the necessary reflection angles to establish the evanescent wave in aqueous medium.

As shown in Table 2.1.2, the main advantage of TIRF is enhanced *Z*-resolution and axial sectioning. The effective *XY* resolution may also be increased, as it benefits from a reduction in background fluorescence. In addition, relative to other techniques such as confocal and two-photon microscopy, a commercial turn-key, objective-based TIRF microscope system is inexpensive. Such a system only requires a microscope, special illuminator(s), lasers, camera, and a high NA objective lens. The main disadvantage of TIRF is related to its main advantage in that only

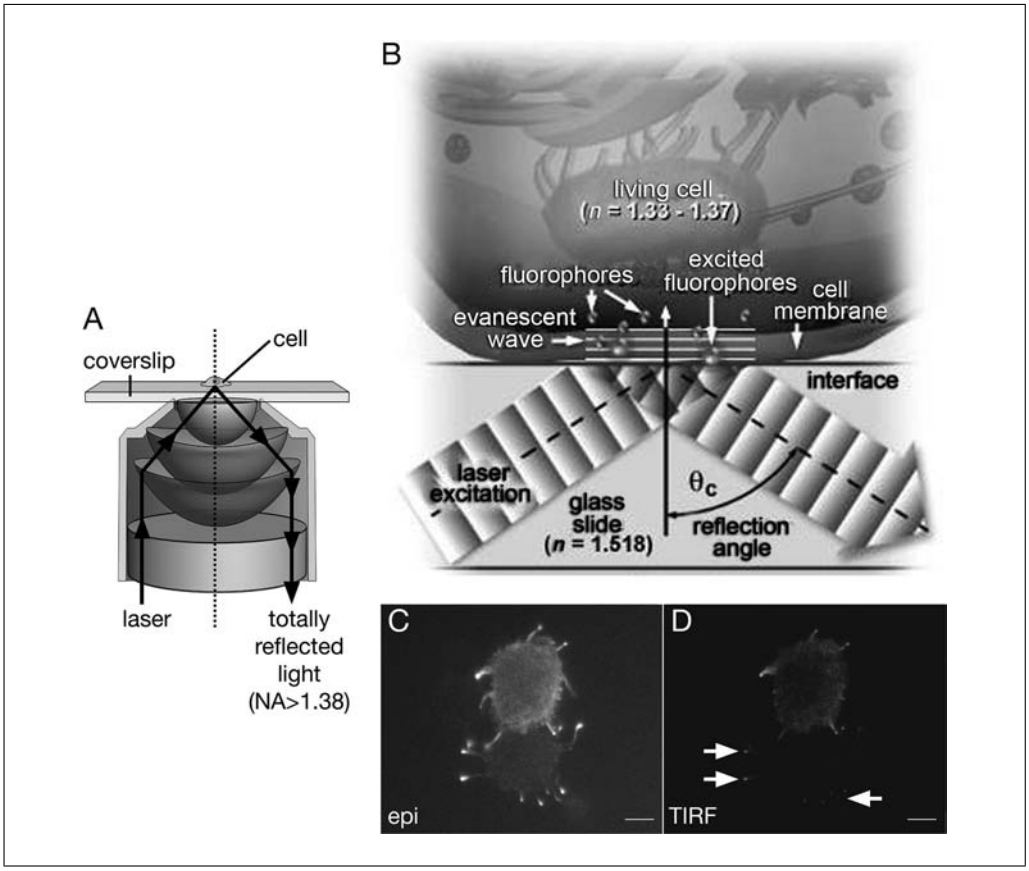

Figure 2.1.2 TIRF microscopy excites a shallow region above the coverslip using oblique laser excitation, which is totally internally reflected and produces an evanescent wave for fluorophore excitation. (**A**) Internal reflection: light propagating through the periphery of a high numerical aperture objective ($>$1.38) is totally internally reflected by the coverslip and sent down the opposing side of the objective. (**B**) An evanescent wave is formed when the critical angle θ_C is reached and the light is totally reflected. The reflection at the coverslip is due to the oblique angle of illumination and the mismatch of refraction index (*n*) between the oil and coverslip. Note that the evanescent wave only excites fluorophores where the cell attaches or is touching the coverslip. **C** and **D** show wide-field and TIRF images, respectively, of GFP-tagged myosin V in two hemocytes from a Drosophila embryo. Comparing the two images it is evident where the Myosin 5 is closest to the coverslip. In the top cell much of the cell is near the coverslip. In the bottom cell only areas in the periphery are near the coverslip (highlighted by arrows). Hemocytes courtesy of Amy Hong (NHLBI, NIH). B was reproduced with permission from Mike Davidson (Florida State University and the National High Magnetic Field Laboratory) and the Molecular Expressions Web site. Scale bars 5 μm in (C) and (D).

fluorophores in the first 200 to 300 nm can be excited. This obviously limits imaging to near the coverslip but enables a *Z*-resolution to the same depth as the penetration of the evanescent wave—typically several times better than confocal microscopy. In addition, because the intensity of the evanescent wave decreases according to this relationship in Eqn. 2.1.2, fluorescence intensity will be a function of distance from the coverslip as well as the concentration of the fluorescent molecules. This makes quantification of depth from the coverslip or comparisons of molecular concentration nontrivial when imaging in TIRF.

CONFOCAL MICROSCOPY

The laser scanning confocal microscope (LSCM) remains a key piece of equipment in most imaging laboratories. Most modern LSCM systems offer hardware and software that automate or simplify complicated experiments such as sequential 3D (*XY* images taken sequentially from top to bottom of the sample, known as a *Z* stack), 4D (*Z* stack over time), or even 5D *Z* stack over time including spectral imaging) experiments. Spectral deconvolution, Fluorescence Recovery after Photobleaching (FRAP), and Fluorescence Resonance Energy Transfer (FRET) procedures are also often included. There have

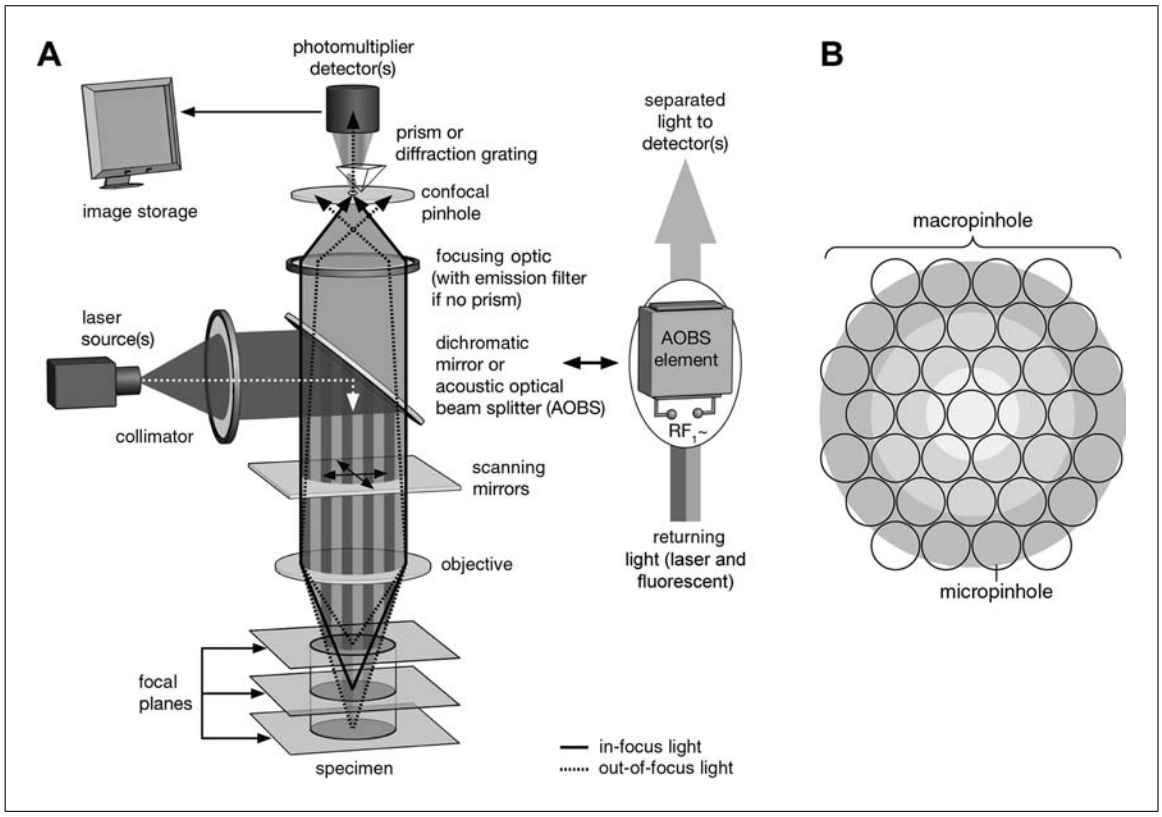

Figure 2.1.3 Basic architecture of a modern confocal microscope. (**A**) Excitation light from laser is passed through the various collimating optics in a scan-head to either a variable dichroic mirror (Nikon, Zeiss, or Olympus and others) or an AOBS (Acousto-Optical Beam Splitter) (Leica) where it is reflected through the objective and focused to a point on the sample. Moveable mirrors (in the scan- head before the objective) scan the excitation beam over the sample a point at a time to build the image. Fluorescence emission light passes back through the objective, through the dichroic or AOBS to the light sensing PMT(s) (photomultiplier tube). An aperture (pinhole) placed in the conjugate image plane to the point of focus in the sample allows only light from the focal plane to impinge on the sample and out-of-focus light is blocked. The pinhole can be made larger to allow for better signal collection—but optical sectioning degrades, as the pinhole allows more out of focus light to impinge on the PMT(s). In some models a diffraction grating or prism placed in the beam-path of the emission light can act as a variable band-pass filter or as a spectral detector if the polychromatic light is spatially spread on a number of PMTs. (**B**) Stylized schematic of subsampling of the emission 2D PSF by either a 32-element detector array (Zeiss Airy Scan) or by multi-focal excitation and subsequent camera based detection (iSIM, see text for details). By sampling with many much smaller pinholes (micropinholes), with the appropriate shifting and summing of the signal one can increase SNR and resolution relative to a single large pinhole (macropinhole) as is employed in conventional LSCM.

been many reviews written about confocal microscopy, but readers are encouraged to consult the following texts for comprehensive information regarding all forms of confocal microscopy, as well as other microscopy techniques (Hibbs, 2004; Pawley, 2006).

In the past few years, many changes have been made to improve confocal microscopes, but the fundamental design for optical sectioning remains largely unchanged. Figure 2.1.3 shows a simplified diagram of the light path of an LSCM. Laser light is directed to the sample through collimating and beam-steering optics, scanning mirrors (which sweep the laser beam over the field of view) and an objective that focuses the light to a diffraction limited spot in the sample.

Emission light from the sample is directed to light-sensing detector(s) [very sensitive photomultiplier tube(s), GaSP detector(s), hybrid detector(s), or camera(s)] through a pinhole that is in the conjugate image plane to the point of focus in the sample. After out-of-focus light is filtered out by the pinhole, the light is sensed by the detectors, and a proportionate voltage is produced, amplified and converted into digital levels for image display and storage.

At the heart of the confocal microscope is the pinhole. When placed in the conjugate

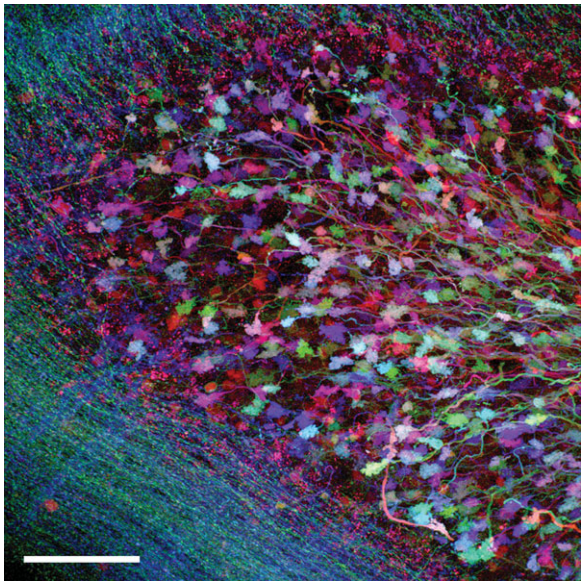

Figure 2.1.4 Maximum intensity projection reconstruction from confocal images obtained through a 65-μm stack of mouse cerebellum labeled with a combination of fluorescent proteins. In the image one can see the unique colors produced and spectrally detected by the genetic combinations of individual fluorescent proteins, which the authors label as XFP's. These colors were used to trace and map the various synaptic circuits. This figure was reproduced with permission from Livet et al. (2007. Scale bar: 50μm.

image plane to the point of focus on the sample it enables optical sectioning (Fig. 2.1.3). The pinhole optically sections by blocking light originating from other focal planes in the sample (out of focus light). Although the pinhole facilitates optical sectioning it must be understood that the *Z* (i.e., axial) resolution is still worse than the *XY* resolution (similar to WFFM). Axial resolution (R_z) in the confocal microscope is approximated by the expression:

$$R_z = 1.4\lambda\eta/(NA)^2$$

Equation 2.1.3

where λ is the wavelength of the emission light, η is the refractive index of the mounting medium, and NA is the numerical aperture of the objective. For instance, green emission light coupled with a pinhole and a high NA lens (oil lens at NA of 1.4) would enable an ideal axial resolution of approximately 0.6 μm (in practice, axial resolution is usually between 0.6 and 1.0 μm). The difference between the *XY* and Z dimensions leads to a resolution limit that is ellipsoidal in shape in 3-D space.

Most LSCM manufacturers also offer a spectral imaging option that will allow for either variable band-pass emission filtering or spectral detection on a per pixel basis. This works by placing either a diffraction grating or a prism in the light path before the detector (s). In many cases, polychromatic (spectral) light is passed to a PMT (photo-multiplier tube) array to detect a range of wavelengths either sequentially or simultaneously depending on the range of wavelengths desired. An example of this type of imaging is shown in Figure 2.1.4 where many fluorescent proteins are simultaneously imaged in a sample. Although this option allows for more versatility and direct selection of the emission range it can come at the cost of less sensitive detection, due to the light loss through the additional optics required and in the spreading out of the light over a series of detectors to enable the spectral detection.

Although LSCM traditionally provides diffraction limited imaging, one can close the pinhole lower than one airy unit to improve the resolution at the expense of signal-to-noise (Pawley, 2006). An airy unit is the width of the zero-order portion of the diffraction pattern (airy disc) at the imaging plane. Recently a new type of image detection system called "Airy Scan" has been introduced by Zeiss (Jena, Germany), which enables almost 2× the diffraction limit in resolution in all three dimensions. This system uses 32 different detectors, which act as very small pinholes to sample the emission airy disc pattern (Fig. 2.1.3B).

By reassigning the light from all the detectors and summing their signal the signal to noise is enhanced and the resolution improved due to the effective pinhole being a fraction of one airy unit. Drawbacks in this scheme include the cost of the detectors, the added processing time and the need to collect 32× more data than a conventional LSCM.

Table 2.1.2 compares the strengths and weaknesses of LSCM. The main advantage of LSCM is the excellent optical sectioning quality, resulting in images with excellent background rejection in moderately thick (<100 μm) samples.

Another advantage is the versatility of imaging capabilities and types of experiments one can perform. Most of these systems have multiple channels for multi-color, variable pinhole sizing for selecting the desired optical section thickness (which allows sacrificing of *Z* resolution for greater signal intensity), and software for variable ROI (region of interest) selection. Another example is the ability to separate spectrally overlapping fluorescent proteins by spectral detection and spectral deconvolution methods (Dickinson, Bearman, Tille, Lansford, & Fraser, 2001). In addition, these systems, particularly in the inverted microscope configuration, can accommodate live or fixed cells or tissue. Many manufacturers also provide options for stage incubation systems. These systems allow relatively long-term experiments, particularly when coupled to automated acquisition software that enables auto- focusing algorithms in tandem with precise *XYZ* stage movement. Disadvantages of a modern LSCM system include the relatively low scan speed (as the beam must be swept through each pixel in the field of view), the relatively high price, and the amount and intensity of light impinging on the sample. The flexibility of the LSCM offsets many of the disadvantages, and one can often balance the imaging variables listed in Figure 2.1.1 to maximize the information content in any given experiment. For instance, if full-frame imaging speed is too slow to capture a physiological event in a live cell experiment one might use a smaller ROI to increase temporal resolution. Despite this flexibility, phototoxicity is always a concern in LSCM when imaging live samples, and must be optimized carefully to avoid damaging or photo-bleaching the sample.

Another type of confocal microscopy is multipoint confocal microscopy, which includes Nipkow spinning disk, swept-field, and slit line scanning microscope systems. Each of these microscope systems shares the characteristic that multiple parts of the sample are imaged at once, thus increasing imaging speed. In the case of the Nipkow spinning disk and swept field systems, a sensitive camera (typically an EMCCD or sCMOS) is also employed. This allows for fast (usually tens to hundreds of milliseconds vs. the seconds timeframe of the LSCM), relatively low-light confocal imaging. Nipkow scanning systems have a drawback in that confocal sectioning can only occur with relatively high NA objective lenses and the pinhole size is fixed or available in only a few sizes based on the objective lens used. These multi-point systems also suffer from crosstalk among pinholes when imaging more than tens of microns into thick samples. Therefore, this class of confocal systems does not allow for imaging as deeply as LSCM systems (Table 2.1.2) (Egner, Andresen, & Hell, 2002). In the case of the slit-scanning confocal microscopes, there is also a modest decrease in resolution in the direction perpendicular to scanning. All of these systems are usually cheaper than a LSCM system but can become relatively expensive if a very sensitive camera is also included.

TWO-PHOTON FLUORESCENCE MICROSCOPY (TPFM)

TPFM is a type of laser scanning microscopy that optically sections inherently and is particularly useful for imaging thick samples both in vitro and in vivo (Denk, Strickler, & Webb, 1990), often out-performing confocal microscopy for samples >100 μm. It has been used to image hundreds of microns into tissues (for reviews, see Diaspro et al., 2006; Svoboda & Yasuda, 2006; Mostany, Miquelajauregui, Shtrahman, & Portera-Cailliau, 2015). An example of this type of imaging is shown in Figure 2.1.5C. Deep imaging is achieved by using pulsed near-infrared excitation light. Infrared light penetrates much deeper into tissue than the visible wavelengths used in standard confocal and wide- field microscopy due to decreased scattering and absorption. This technique is also good for limiting the excitation (and often photo-bleaching and possible photo- toxicity) to just one focal plane, since excitation is mostly confined to the region of highest intensity (the focal spot). This also has the added benefit of eliminating the need for a pinhole aperture for optical sectioning as is used in confocal microscopy. In confocal microscopy the pinhole is used to reject out-of-focus emission light from reaching the photo-sensor (photo-multiplier tube or camera). In effect, the pinhole selects only a

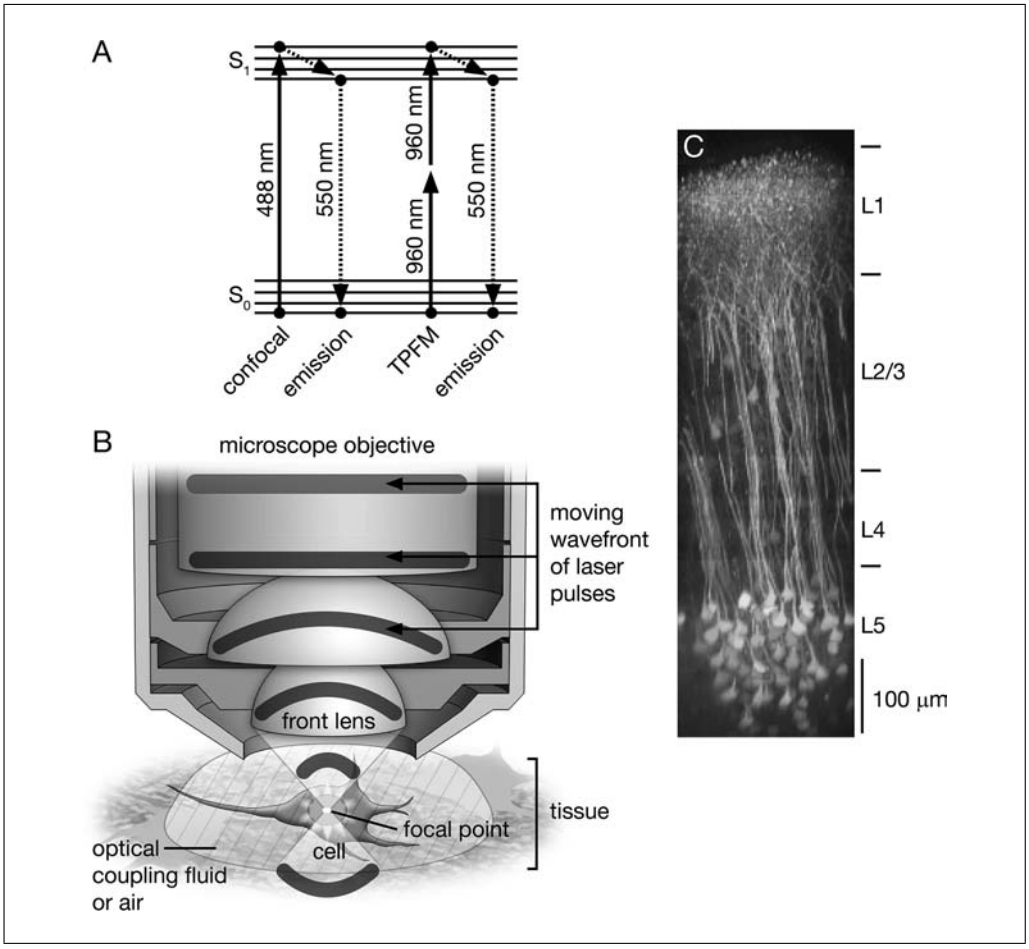

Figure 2.1.5 Principles of two-photon fluorescence microscopy (TPFM) and example image. (**A**) Shows a regular one-photon (e.g., confocal) and TPFM energy transitions in a Jablonski diagram. In TPFM two photons are absorbed nearly simultaneously to produce twice the energy. In this example GFP is excited with 960-nm light for TPFM and 488-nm higher energy light for a confocal experiment. The emission is the same for both cases. TPFM absorption spectra for most fluorophores, including GFP, are very broad (in some cases hundreds of nanometers), and the maximum is roughly a little less than twice the one-photon absorption maxima. (**B**) Two-photon fluorescence is generated in only one plane when a laser pulse train propagating through an objective is focused to a spot. Fluorescence is generated only at the point where the maximal photon crowding occurs and falls off from this plane at a rate of the fourth power from the center of the focal spot. (**C**) In vivo TPFM image of a mouse neocortex genetically labelled with a chloride indicator. This image shows the remarkable depth to which TPFM imaging is possible. C is reproduced with permission from Helmchen and Denk (2005).

small portion of the emission light to achieve optical sectioning with much of the emission light "thrown away." In TPFM it is the excitation pulse that provides the optical sectioning; therefore, much more of the light can be collected from the excited focal spot and far fewer scattered or ballistic emission light photons need be wasted during collection. TPFM is a form of multi-photon imaging. Multi-photon imaging refers to techniques where more than one photon at a time is used to excite a fluorophore.

TPFM excitation occurs when a fluorophore absorbs two photons essentially simultaneously. This roughly doubles the amount of energy absorbed by the fluorescent molecules which drives their excited electrons to the same energy level as would the absorption of one photon at approximately one-half the two-photon excitation wavelength (Fig. 2.1.5A). An example would be the excitation of GFP (typically excited using 488 nm using a CW (continuous wave) laser in a confocal experiment) at around 960 nm using a pulsed laser. The doubling of wavelength in TPFM is an oversimplification, as the actual TPFM absorption spectra for many fluorophores are over 100 nm broad, and "selection rules" that govern the relative strengths of absorption bands vary between one-photon

and two-photon excitation, but in most cases doubling the 1P (one-photon) wavelength is a good starting point for estimating where TPFM excitation occurs. The broad spectral absorption range of the typical two-photon fluorophore allows for multiple fluorophores in a sample to be excited at one wavelength simultaneously. Corresponding emission wavelengths for each fluorophore are then separated in different channels with the appropriate dichroic and emission filters or with spectral detection. The inherent optical sectioning ability of two-photon excitation arises due to the increased probability of two-photon absorption that occurs at the diffraction limited spot due to spatial energy crowding (Fig. 2.1.5B). This can be seen in the equation for time averaged two-photon fluorescence intensity (I_f):

$$I_f \approx \delta_2 \eta (P_{ave}^2/\tau_P f_P)(NA^2/hc\lambda_{exc})^2$$

Equation 2.1.4

where δ_2 is the two photon cross section for the fluorophore, η is the quantum yield of the fluorophore. P_{ave} is the average power of the excitation beam, τ_P is the pulse width of the excitation pulses, f_P is the repetition rate of the laser, NA is the numerical aperture of the objective, h and c are Planck's constant and the speed of light respectively, and λ_{exc} is the wavelength of the excitation light (Diaspro et al., 2006). In fact, the probability of two-photon absorption decreases as the fourth power of distance away from this focal region along the Z-axis (as can be seen by the NA dependence in Eqn. 2.1.4) and increases as the square of the intensity (mW of power are typically required). Another variable is the temporal pulse width, τ_P, of the excitation light pulse as it reaches the sample. In general, short pulse widths (on the order of 100 fsec) are optimal for two-photon excitation.

Second Harmonic Generation (SHG) imaging is another multi-photon technique often used in conjunction with TPFM on commercial microscopes. SHG is a coherent scattering process that occurs when a pulsed laser is used to illuminate certain ordered molecules, such as collagen, microtubules, and myosin (Campagnola & Loew, 2003). SHG requires no fluorophore and the scattered photons are collected at exactly twice the excitation frequency (half the excitation wavelength). It is often used to show structural features in biological samples. It can also be an unwanted signal that confuses interpretation of TPFM images if the bandwidth of the emission filter includes ½ the excitation wavelength.

Commercially available turn-key TPFM systems usually consist of a modified point-scanning confocal microscope, which includes a Ti:Sapphire pulsed laser (tunable over a broad range of wavelengths) and nondescanned detector channel(s). The nondescanned detector is mounted on the microscope in a position that is close to the sample, so that the emission light does not travel back through the scan-head. Since no pinhole is necessary, this configuration can be employed to reduce light losses that would occur if the emission light passed back through the scan-head. Typically, commercially available pulsed lasers produce approximately 100 fsec pulses at a rate of 80 MHz. Dispersion in the optics of the microscope and objective will lengthen these pulse widths by at least a factor of two, thus lowering the probability of excitation at the sample (see Eqn. 2.1.4). Some commercial lasers now optionally include an additional unit for pre-compensation of this dispersion which can reduce the pulse length at the sample and thus restore two-photon fluorescence efficiency.

Planning for a TPFM experiment requires more than just the knowledge encoded in Eqn. 2.1.4. One consideration is that more care may need to be taken for dye separation in multi-color experiments where multiple fluorophores may be excited with the same two-photon excitation wavelength. This can be done with band-pass emission filters or spectral un-mixing (available on most modern microscopes). Many fluorophores and fluorescent proteins have good cross-sectional area for two-photon microscopy (Spiess et al., 2005; Drobizhev, Makarov, Tillo, Hughes, & Rebane, 2011; Mütze et al., 2012) and careful consideration of their spectral properties before an experiment can avoid spectral cross-talk. Also, in general, more red- shifted IR wavelengths will allow for deeper imaging with less photo-damage (Kobat et al., 2009), although the absorption of water and the potential for slight sample heating have to be considered for wavelengths above 1200 nm. Optical Parametric Oscillators (OPO) and some lasers can tune to wavelengths >1000 nm. This has the added benefit of being able to excite red-shifted fluorescent proteins that may not be easily excited with a standard Ti:Sapphire laser (Vadakkan, Culver, Gao, Anhut, & Dickinson, 2009).

In summary, as is shown in Table 2.1.2, the main advantage of TPFM is the depth of imaging (hundreds of microns) into the sample.

Another important advantage is that bleaching and phototoxicity are limited to the focal plane; however, in the focal plane the damage can be greater due to the higher excitation power (time averaged power of mW compared to μW in confocal; 10^5 higher peak power at the focal spot) needed for TPFM. TPFM typically requires the same time frame for acquisition as traditional LSCM (on the order of 1 sec/frame). Relative to wide-field microscopy, disadvantages are the costs associated with a point- scanning microscope (a trait shared by laser scanning confocal microscopy) and a tunable pulsed laser system. The cost increases if one also adds a precompensation unit to correct dispersion in excitation pulse lengths or selects the correct laser(s) or OPO to extend the wavelength ranges for excitation above 1000 nm.

STRUCTURED ILLUMINATION FLUORESCENCE MICROSCOPY (SIM)

Structured Illumination Microscopy (SIM) encompasses a range of techniques that can enhance optical resolution and/or optical sectioning with potentially less light, higher temporal resolution, and less cost than other techniques. SIM also works with many more fluorophores than, for example, stimulated emission depletion (STED) and localization microscopy super- resolution techniques (described in other sections of this manuscript). SIM was pioneered for biological imaging by Wilson and colleagues (Neil, Squire, Juskaitis, Bastiaens, & Wilson, 2000) (for optical sectioning) and Mats Gustafsson (Gustafsson, 2000) (for super-resolution). To understand SIM it is necessary to understand how patterned

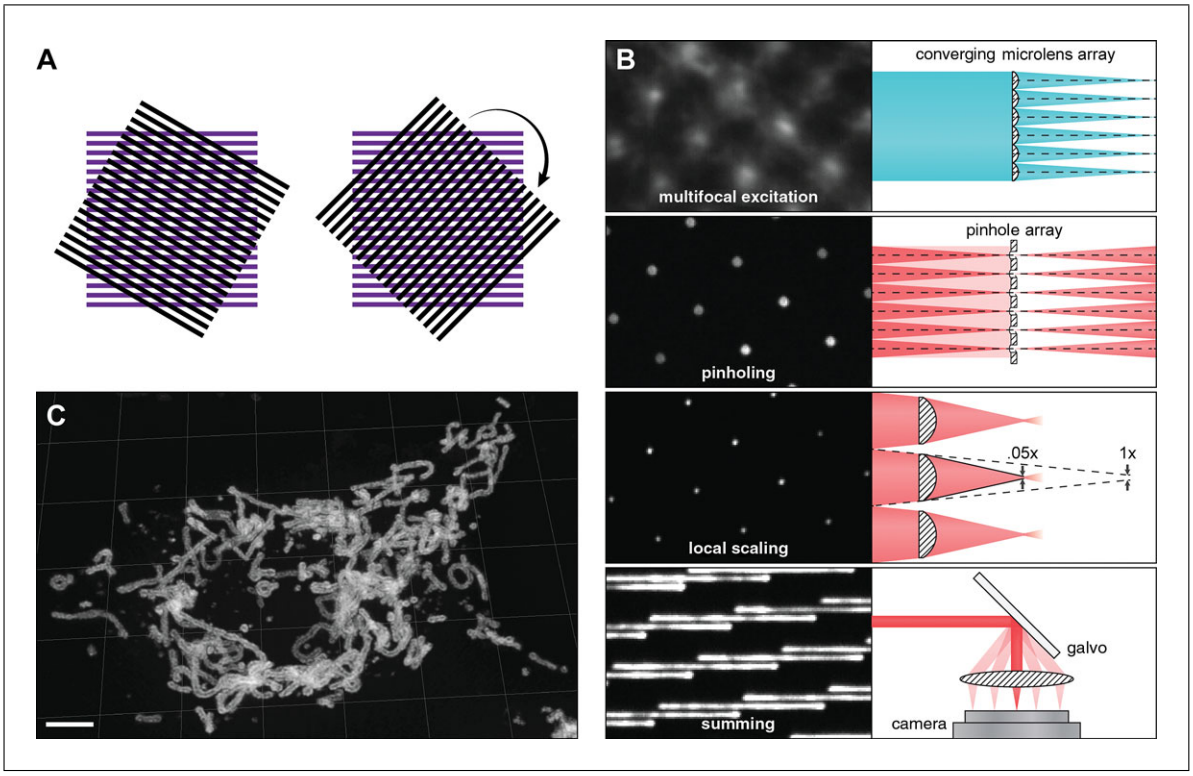

Figure 2.1.6 Two imaging modalities for Structured Light Microscopy (SIM) and example image. (**A**) Schematic showing principles of traditional SIM. If an unknown pattern (such as a biological sample) is multiplied by a known regular illumination pattern (here the two patterns are shown as simple overlaid grids) then a beat pattern (moiré fringes) will appear. The beat pattern is coarse enough to be seen through the microscope even if the original pattern in the sample was not resolvable. By rotating (right) and phase-stepping the pattern relative to the sample and computationally processing the resulting data, an image can be generated that has resolution approximately 2× better than a conventional wide-field image. (**B**) Schematic outlining the steps to produce super-resolution SIM (SR-SIM) imaging using the techniques iSIM (Instant SIM). Multifocal excitation spots are generated through a series of microlenses and the resulting emission passes through pinholes and microlenses for scaling. When quickly swept over the sample, the effect is to produce a super-resolution SIM image without the need for processing (see text for more details). (**C**) Maximum intensity projection derived from volumetric ISIM image of cultured fibroblast cells expressing the outer mitochondrial membrane protein TOM-20 labelled with neon-GFP (courtesy of the NHLBI Transgenic Core). Note the clearly defined mitochondrial outer membranes. This image was deconvolved using Microvolution deconvolution software (Menlo Park, CA). Scale bar: 3μm.

excitation light can interact with a sample to enhance spatial resolution. Figure 2.1.6A shows how two patterns can mix to produce new patterns known as moiré fringes. SIM relies on measuring the spatial frequencies produced by the interaction of the known patterned illumination with the spatial frequencies inherent in the sample, and solving for the underlying spatial frequencies present in the sample. If the excitation pattern is diffraction-limited (as sharp as possible), resolution enhancement up to ~twice the diffraction limit is possible. To produce the final SIM image with equivalent resolution improvement in all dimensions it is usually necessary to rotate and/or phase shift the excitation pattern; the number of rotations and/or phase shifts depends on the details of the hardware and the algorithm used to produce the SIM image. An alternate method of understanding the same effect is to consider the resolution enhancement that results when a diffraction limited excitation pattern (producing fluorescence) is multiplied by the emission point-spread function at each location in the sample—the effect is analogous to the extension in frequency space that is possible when the excitation pattern "mixes" with the underlying spatial frequencies in the sample. We emphasize that this method of resolution enhancement can be produced in different ways; accordingly, commercially available microscopes differ in the speed they offer, amount of applied light, and the depth penetration in which high spatial resolution can be produced.

In its simplest form, a camera based wide-field microscope with an arc—lamps or LED based light engine can be modified with a moveable grid pattern in the excitation path to produce optically sectioned SIM images. Multiple images (as few as three) are acquired as the pattern is moved, and then optical sections are created by using a simple mathematical formula to analyze the way in which detected fluorescence from the sample interacts with the pattern. This procedure can produce images with axial resolution and optical sectioning approaching that of a confocal based microscope system.

Part of the revolution associated with super-resolution, SIM (SR-SIM), and now available commercially in several microscope designs, has also been in breaking the diffraction barrier (Gustafsson, 2000; Schermelleh et al., 2008). One common commercial design uses laser light and a grating to produce a fine structured illumination pattern in a camera-based microscope. The illumination pattern is varied (rotated and phase stepped), multiple images are acquired (~10 to 100/slice), and a composite super-resolution image is produced computationally from the underlying raw data. A second method, instant structured illumination microscopy (iSIM): (1) scans multiple diffraction-limited excitation foci (a form of "structured illumination" produced with a microlens array similar to that in spinning disk microscopy) across a sample; (2) uses a matched pinhole array to reduce out-of-focus light; (3) employs a second, matched microlens array to perform analog image processing on each fluorescent foci, thereby improving image resolution; and (4) integrates the resulting fluorescent foci to produce a final image, with $\sqrt{2}$ improvement in spatial resolution, onto a sensitive camera (Fig. 2.1.6B and 6C) (York et al., 2013). This technique has the advantage that the super- resolution image is formed optically without the need for processing. Super- resolution images can be formed at the frame rate of the camera (hundreds of images/sec), limited in practice only by the required signal-to-noise ratio. A full increase of twice the diffraction limit is achieved with deconvolution.

The main disadvantage of traditional SIM is the computational and acquisition time necessary to obtain the final image. Blurring or reduction in resolution can occur if the sample moves during the time necessary to take multiple images. Depth penetration into thick samples can also be problematic, as traditional SIM is based on a wide-field microscope and is thus prone to shot noise contamination from out-of-focus light originating elsewhere in the sample. In general, much like localization microscopy, the depth is limited to approximately 10 μm into most biological samples. iSIM, described in the previous paragraph, has been shown to go much deeper and can reach depths $>$100 μm when combined with multiphoton excitation (Winter et al., 2014; Winter et al., 2015) and is much faster (York et al., 2013) than traditional SIM.

STIMULATED EMISSION DEPLETION (STED) FLUORESCENCE MICROSCOPY

STED microscopy is a super-resolution optical technique that can improve fluorescence microscopy resolution by approximately an order of magnitude over traditional diffraction limited techniques, such as LSCM. Super-resolution images are produced without the need for post-processing (although

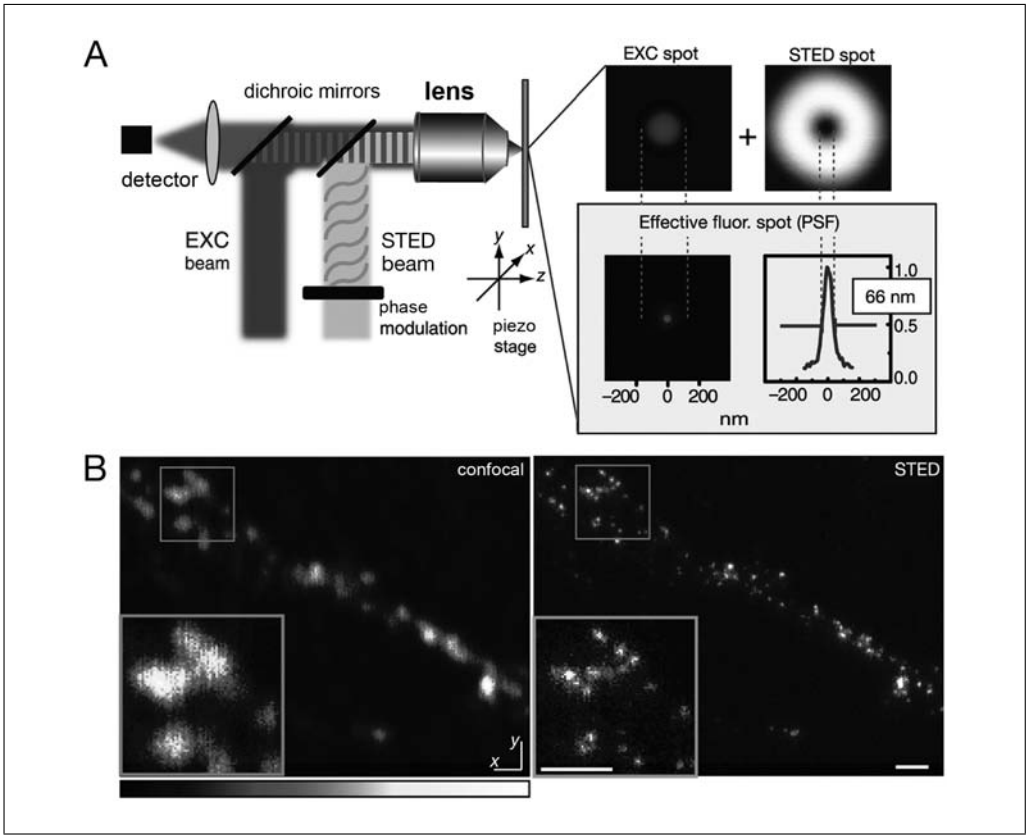

Figure 2.1.7 Technical principles of Stimulated Emission Depletion (STED) microscopy and example image. (**A**) The combination of the normal excitation beam with the donut shaped STED beam produces a sub-diffraction emission spot. The images on the right in (A) show the donut STED beam. When overlapped with the diffraction-limited excitation spot, the STED beam quenches emission where the beams overlap, leaving fluorophores in the middle, sub-diffractive spot available for spontaneous fluorescence. Panel A reproduced with permission from Willig et al. (2006). (**B**) Confocal image of Caco-2 cells labeled with Alexa 647 (ZO-1 tight junction protein, red) and Alexa 594 (cingulin tight junction protein, green). (**C**) STED image of the same cells as in (B). The STED image was acquired for both fluorophores using a 775-nm depletion laser. Note the increase in resolution in the STED image showing that ZO-1 is in the middle of two zones of cingulin. Images in (B) and (C) courtesy of Christina van Itallie (NHLBI, NIH). Scale bar: 1μm.

deconvolution can provide additional gains in resolution and signal-to-noise). This technique can provide a level of resolution on biological samples surpassed only by single- molecule localization microscopy (described below), and – since it is based on a confocal geometry and faster than single-molecule localization microscopy- can be more versatile for live-cell or 3-D imaging (Willig, Rizzoli, Westphal, Jahn, & Hell, 2006; Kellner, Baier, Willig, Hell, & Barrantes, 2007). STED improves resolution by a direct reduction in the effective emission spot size: a second laser beam is used to force fluorophores in the periphery of the conventional diffraction-limited excitation spot to undergo stimulated emission (effectively out-competing spontaneous fluorescence and thus quenching fluorescence in this region, see also Figure 2.1.7 and further discussion below). It is important to note that the improvement in resolution is achieved directly without the need for post-processing. STED is so straightforward that to the user it seems little more different than a normal point-scanning technique, such as LSCM or TPFM. Due to patent considerations Leica Microsystems (Wetzlar, Germany) was initially the sole provider of commercial systems, but now other companies (e.g., Abberior GmbH) are selling STED systems as well.

Figure 2.1.7A shows a simplified optical setup for the STED technique. Super- resolution is achieved by exciting the fluorophore as would normally occur in a LSCM experiment and then quenching the fluorescence in a spatially selective manner by using a second, longer wavelength "STED" laser. Specialized optics in the scan-head alter the phase of the STED beam wave-front so that a donut pattern (with a node at the central portion of the

donut) is created at the focal spot. The STED wavelength must be red shifted (longer wavelength) such that it does not overlap the absorption spectrum of the fluorophore but does overlap its emission spectrum (usually at the tail-end to allow for maximal emission bandwidth). In this way, it effectively quenches the emission of the fluorophore in the area of the spot where the STED beam overlaps the excitation beam (forces the excited electrons into the ground state, which concurrently results in the stimulated emission of light at the same wavelength as the STED beam). This reduces the size of the emitting region to that of the middle of the doughnut. The size of this region is inversely related to the power of the STED beam according to the following expression:

$$R \approx \lambda / \left(2NA\,(1+\zeta)^{0.5}\right)$$

Equation 2.1.5

where R is the lateral (*XY*) resolution, λ is the wavelength of the excitation light, NA is the numerical aperture of the objective, and ζ describes the saturation factor of the STED beam. ζ is the ratio of the intensity of the STED beam (I) to the intensity at which ½ of the fluorescence is effectively quenched (I_{sat}). It is important to note that each fluorophore has a different saturation factor and thus a different relationship between the power of the STED beam and achievable resolution. The point-spread-function (PSF) engineering in STED can also be altered to improve axial resolution by using additional optics to form a donut in the *Z* dimension, thereby squeezing the effective emission spot in three dimensions.

In this manner, commercial STED microscopes can produce images with resolution around 50 nm in plane and 100 nm in the *Z* dimension, and in some cases STED imaging can improve resolution to less than 40 nm (Willig, Harke, Medda, & Hell, 2007; Schmidt et al., 2008).

In practical terms the most important consideration in a STED experiment is the choice of the fluorophore (dye or fluorescent protein) to be imaged. Outside of biological considerations this choice will be restricted by the wavelength and type of STED laser used (pulsed or continuous wave) and the number of colors to be imaged. In general fluorophores with a lower I_{sat} and those that are more resistant to bleaching are the best choices. Typically, more red-shifted fluorophores that use red-shifted STED lasers produce better obtainable resolution with less photo- damage and bleaching (CA Combs, person. observ.). In terms of the STED laser, pulsed-lasers quench fluorescence much more effectively and can produce greater enhancement of resolution at lower powers than continuous wave lasers (Willig et al., 2007). Time-gating the emission collection can also reduce the amount of STED power needed, particularly when CW lasers must be used (Vicidomini et al., 2013).

Two-color STED can be performed by either using different STED beam wavelengths or by using the same wavelength for both color channels. Care must be taken when using different STED wavelengths as the blue-shifted STED beam of one color channel can usually be absorbed and rapidly bleach the red shifted fluorophore in the dual color experiment (Pellett et al., 2011). For fixed samples, this problem can be avoided by imaging the red channel first, but for live experiments such an approach can be problematic. Using the same STED beam for both fluorophores can circumvent this problem (Pellett et al., 2011). An example of this approach uses a 775 nm STED beam for the dye pairs Alexa 594/Sir dye (New England Biolabs and Spirochrome) or Alexa 594/Alexa 647 (Molecular Probes). Leica has an online guide to sample preparation that includes most of the best fluorophores for STED and makes recommendations for dye pairs for multicolor experiments (*http://www.leica-microsystems.com/science-lab/quick-guide-to-sted-sample-preparation/*).

The main disadvantages of the STED approach are the cost of the system and the amount of power that impinges on the sample (Table 2.1.2). The cost of the system is relatively high due to the need for powerful STED depletion lasers and for the additional optics necessary to create the doughnut beam(s). Time-gated hybrid detectors can add to the system cost, as can auto-aligning hardware.

Another disadvantage is that the amount of power used in a STED system is high (tens of mW average power for the second beam). Since there is the potential for destruction of the probe or sample, only very photostable fluorophores can be used. Maintaining the shape of the STED beam with depth is also sample dependent; the donut beam for 3D super-resolution imaging is particularly sensitive to depth-dependent aberrations. In brain, super-resolution with STED has been shown to a depth of approximately 80 μm (Urban,

Willig, Hell, & Nagerl, 2011). This is considerably better than what is routinely achieved with fluorescence localization techniques such as PALM and STORM. As with other super-resolution techniques, movement of the sample during the imaging period will degrade resolution, and can be particularly problematic for relatively slow, point scanning techniques such as STED. Resonant scanners can image at tens of frames/sec and may help, although obtaining an acceptable SNR over the resulting, ultrashort dwell times may be difficult or impossible – in which case other techniques (such as iSIM) may be a better choice in attempting to resolve high speed phenomena below the diffraction limit (York et al., 2013).

SINGLE-MOLECULE LOCALIZATION FLUORESCENCE MICROSCOPY TECHNIQUES (SMLM)

In practice, SMLM techniques provide the highest resolution (in some cases, down to ~10 nm) of the various super-resolution techniques currently commercially available, and can be implemented at less cost. SMLM imaging is accomplished by serially localizing the positions of many individual fluorescent molecules to a precision better than the diffraction limit, rather than by directly resolving sub-resolution features (Fig. 2.1.8). This approach can provide lateral resolutions on the order of 10 nm (for limits of resolution and

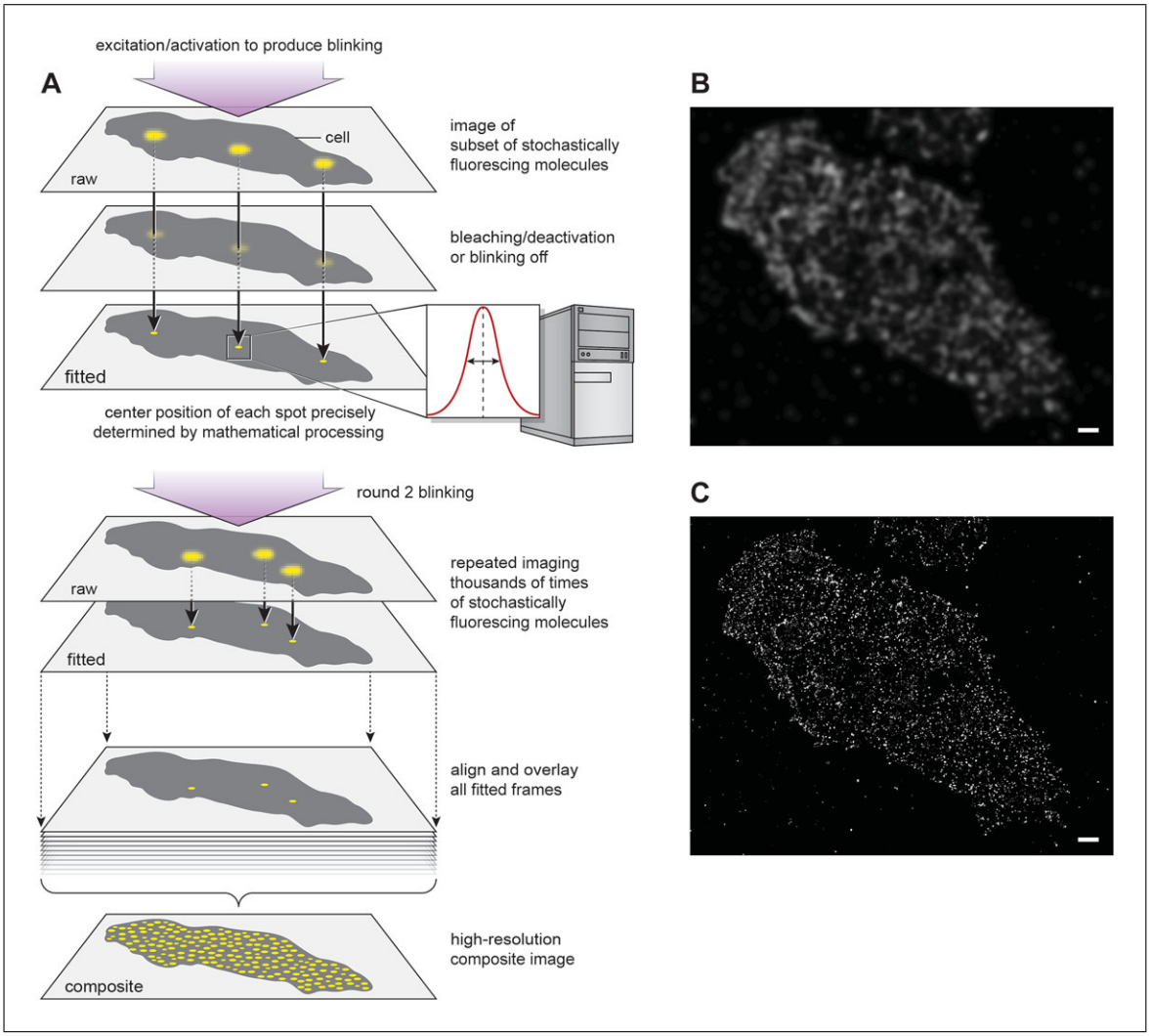

Figure 2.1.8 Basic principles of Single Molecule Localization Microscopy (SMLM) and example image. (**A**) Schematic illustrating the repeated process of imaging the activation and deactivation of stochastically fluorescing molecules in the sample over many thousands of images to build up a super-resolution image after image processing. Simulated wide-field image (**B**) and STORM image (**C**) of INS-1 beta cells expressing the membrane protein Syntaxin-GFP labeled with the GFP- nanobody and Alexa647 label. The protein makes small nanoclusters in the membrane that are below the diffraction limit. Courtesy of Justin Taraska (NHLBI, NIH). Scalebars 1μm in (B) and (C).

review, see Thompson, Larson, & Webb, 2002; Patterson, Davidson, Manley, & Lippincott-Schwartz, 2010) and can be implemented relatively simply using a wide-field or TIRF microscope and a camera. In practice, this approach requires that single molecules are isolated and imaged with no (or minimal) overlap of individual PSFs. This is accomplished by ensuring that only a sparse, optically resolvable subset of fluorescent molecules (usually a stochastic subset of molecules in each frame) is allowed to glow in any individual image; recording a large number of consecutive images (typically many thousand); and identifying and localizing all molecules within the dataset (often by fitting the intensity distribution of each fluorophore to a theoretical point spread function).

The final super-resolved image is then composed by rendering the locations of all fitted points. Sparsity is achieved by turning fluorescence "on" using photo- conversion or photo-activation and then "off" by photo-bleaching bleaching or photo-conversion into a dark state. The localization precision in each dimension is proportional to

$$\mathrm{FWHM_{loc}} \sim \mathrm{FWHM}/(\mathrm{N})^{0.5}$$

Equation 2.1.6

where N is the number of detected photons and FWHM (full-width half-maximum) is the dimension of the diffraction limited PSF measured. From this expression it is clear that the localization precision depends strongly on the brightness of the sample—which can be improved by using high NA objectives, sensitive cameras, and bright probes. In practical terms, however, the most important factor in achieving super-resolution in SMLM is the density of the fluorescent labelling.

The hardware and imaging techniques mean little if the proteins or biological structures of interest are not labeled with sufficient density; in such a case the final image is usually very noisy and structures appear "pointilistic."

There are now many different types of SMLM techniques that are commercially available. These include PALM (Betzig et al., 2006), FPALM (Hess et al., 2006), STORM (Rust et al. 2006), and GSDIM (Folling et al., 2008).

Historically, PALM and its variants have been associated with photo-activation and bleaching (or conversion to a dark state) of fluorescent proteins (and expression of these tags), while STORM has been associated with photo-switching of organic dyes, such as the cyanine derivatives, and standard immunohistological labeling. GSDIM, also known as direct- or dSTORM, relies on using intense laser light to switch off dyes by forcing most of the molecules into a long-lived dark state with intense laser light and then measuring the signal emitted by the relatively few molecules that stochastically return to the ground state. PAINT (Point Accumulation for Imaging in Nanoscale Topography) is a technique that mitigates the problem of low labelling density by adding low concentrations of fluorescent probes directly to the medium (Sharonov & Hochstrasser, 2006). These probes diffuse around the sample and fluoresce upon stochastically binding their target of interest on the surface of cells. Oblique illumination (e.g., at or below the critical angle) that can be implemented in a TIRF microscope limits the zone of excitation and is helpful in reducing background fluorescence, as is TIRF. Although these techniques vary somewhat in their optical configurations and the manner in which they randomly activate fluorescence from sparse subsets of fluorophores they all rely on determining the positions of non-overlapping single fluorophores to a precision better than the diffraction limit in order to build up a composite super- resolved image derived from many single diffraction-limited images.

One of the main limitations of SMLM techniques is the large number of images that are needed to fully define a single super resolution image. The constraints of temporal resolution coupled with the need for organic dyes (as in STORM) and harsh reducing agents (GSDIM) limit the majority of applications to fixed samples. Although processing time and data storage remain concerns in implementing SMLM, the ready availability of fast algorithms (e.g., QuickPalm, (Henriques et al., 2010)) and relatively cheap, large- volume data drives continue to help. Another limitation is that, at least commercially, SMLM is currently limited in depth penetration to sample thicknesses within 10 μm of the coverslip surface (within ~250 nm when implemented on a TIRF microscope). This limitation arises due to the presence of out-of-focus background in thick, densely labeled samples—which can be mitigated if SMLM is performed on a microscope with optical sectioning (i.e., not a wide-field microscope).

LIGHT SHEET FLUORESCENCE MICROSCOPY (LSFM)

In LSFM, excitation (a thin sheet of laser light) and emission occur in an orthogonal configuration (Fig. 2.1.8A) using two perpendicular objective lenses (Huisken, Swoger, Del Bene, Wittbrodt, & Stelzer, 2004; Keller, Schmidt, Wittbrodt, & Stelzer, 2008). Fluorescence excited by the light sheet (and originating from a single plane in the sample, coincident with the detection objective's focal plane) is captured using a sensitive camera. The light sheet is then swept relative to the sample (or the sample is moved relative to the light sheet) to build up an imaging volume. This excitation and emission geometry has many advantages over traditional confocal microscopy methodologies, including much faster 3-D imaging and more efficient excitation (i.e., using less intensity and causing far less bleaching/phototoxicity), while still enabling subcellular resolution and optical sectioning. To date most imaging using LSFM has been done on relatively large samples, such as Drosophila, *C. elegans*, mouse, and zebrafish embryos, where 3-D time-lapse imaging at low excitation power is important. The relatively recent advent of DiSPIM (Wu et al., 2013) and Bessel Beam Plane Illumination and Lattice Light Sheet Microscopy (Chen et al., 2014), both discussed below, have significantly improved the spatial resolution, thus permitting a larger range of samples that can be imaged effectively using LSFM.

Currently, there are many commercial sources for LSFM systems. Here, we simplify their classification into three main types based on beam-path geometry, the way the excitation light-sheet is generated (one-sided and two-sided), and the light-sheet's pattern and thickness. The choice of a system should be based on the size of the sample, how a sample is to be mounted (in agarose or on a coverslip), and the required resolution. For larger samples (such as whole organisms, or whole embryos), agarose mounting and horizontal/vertical configuration of detection and illumination objectives are often used (Fig. 2.1.9A). Here, a light sheet is generated with a low magnification (2.5 to 10×), low NA (typically 0.1 to 0.3) objectives, and emission is collected orthogonally with a water immersion or cleared tissue refractive indexed matched objective coupled to a fast sensitive camera (Fig. 2.1.9A). The sample sits in agarose in a holder (often in a capillary) that is bathed in medium and translated in multiple dimensions through the light sheet to generate a volumetric image. The OpenSPIM project (*http://openspim.org/Welcome_to_the_OpenSPIM_Wiki)* offers complete instructions and parts list for building this type of SPIM *de novo*. A second general type of configuration is shown in Figure 2.1.9B where the objectives are mounted above the sample, thereby allowing the sample to be mounted on a coverslip. An example of this class of LSFM is the Dual-View Selective Plane Illumination (diSPIM) scheme where two symmetric arms terminate in long working distance water immersion objectives (usually 2 40 ×, 0.8 NA lenses) mounted above the sample (Wu et al., 2011; Wu et al., 2013; Kumar et al., 2014)(Fig. 2.1.9B). During imaging, the beam paths are used for light sheet excitation / fluorescence detection in an alternating duty cycle. Images are collected from both beam-paths and combined (via registration and subsequent joint deconvolution (Ingaramo et al., 2014)) to construct an image with isotropic resolution (∼330 nm in ideal conditions) in three dimensions. An example of this type of imaging is seen in Figure 2.1.9C. One recent enhancement allows for a third light path, with imaging from below by a third objective, for greater light collection (Wu et al., 2016)

LSFM on an inverted microscope has also been accomplished using mirrors mounted on either side of the sample (Leica Microsystems, Wetzlar Germany).

Excitation light is focused from below onto mirrors on the emission collection objective. The mirrors surround the sample on two sides. These mirrors combined with scanned laser excitation produce the light sheet. This feature also allows excitation from both sides of the sample, thus reducing the chance for striping due to absorbance of laser light from one side of a sample (Huisken & Stainier, 2007). Fluorescent emission is then collected from above using a second objective. This configuration also allows switching to the conventional confocal mode of imaging in the epi-fluorescence direction using the same lasers and excitation used to generate the light sheet, thereby increasing the flexibility of the device.

A third type of LSFM, available commercially, changes the excitation pattern to produce an effectively thinner light sheet (thus enabling higher resolution). This is accomplished by altering the shape of the excitation profile through patterned illumination at the back aperture of the objective. Using this patterned illumination, a light sheet can be

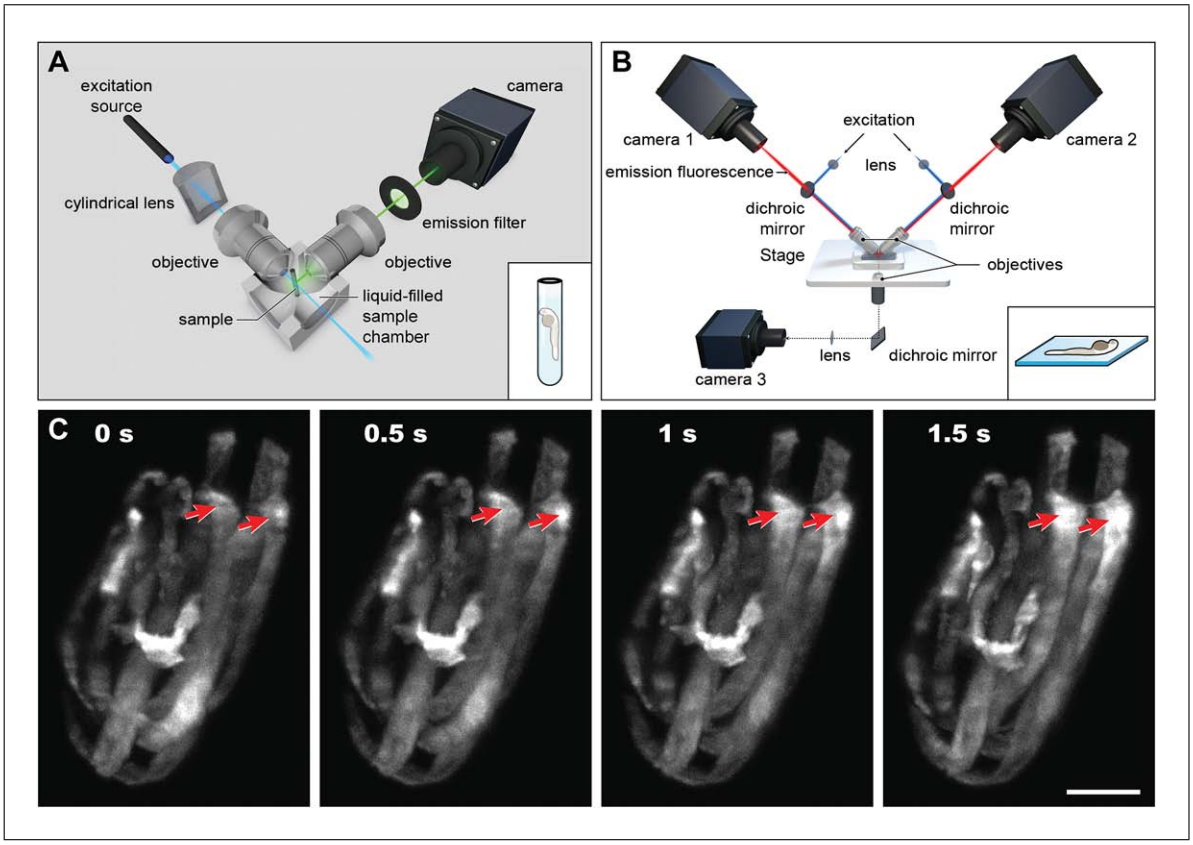

Figure 2.1.9 Light sheet fluorescence microscopy (LSFM) basic architectures and example. Schematic of traditional horizontally based (**A**) and iSPIM based (**B**) LSFM imaging geometries. Note that that the iSPIM geometry allows for imaging the sample on a conventional coverslip on an inverted microscope, while in the traditional geometry the sample sits in a holder, typically in agarose. (**C**) Calcium flux in a late-stage 3-fold nematode embryo, as visualized by iSPIM. GCamp3 was targeted to embryonic muscles and imaged using iSPIM. 50 planes/volume were collected at 5 msec/image; volumes were collected every 0.5 sec for ~500 imaging volumes; no bleaching or phototoxicity was evident even after this prolonged imaging series. Note the onset of a calcium wave indicated by the red arrows. Scale bar: 10 μm. Image courtesy of Evan Ardiel (NIBIB).

produced using multiple beams for a "lattice light sheet" (Chen et al., 2014). These LSFM implementations are well suited for live-cell experiments where sub-cellular resolution and low photo- toxicity over time are desired, although some caution should be applied as patterning the illumination also results in unwanted excitation above and below the focal plane (causing increased bleaching and out-of-focus haze compared to conventional light sheet illumination), and such patterns are very sensitive to aberrations in the sample. The patterning of the light sheet can also be used for super-resolution via SIM methods (discussed above).

One limitation regarding LSFM arises due to the sample itself. Biological structures can absorb or scatter the excitation light, causing shadowing along the length of the sheet. These can appear as streaks or holes in the image. This problem can be ameliorated by excitation from both sides of the sample, as with the Leica patented mirror configuration; via multi-view fusion (using, e.g., the diSPIM); or by dithering the angle of the beam (Huisken & Stainier, 2007). Furthermore, fluorescence—which is usually collected in a wide-field (or perhaps partially confocal) manner—is also sensitive to scattering, absorption, or specimen induced aberrations. For very thick, densely labeled samples, TPFM thus out-performs LSFM.

Another issue to consider in implementing LSFM is the specimen preparation – the requirement for agarose or FEP (Fluorinated Ethylene Propylene tubing; Kaufmann, Mickoleit, Weber, & Huisken, 2012) for some implementations of LSFM, or the steric hindrance caused by the close proximity of the objectives in the inverted platforms. These are additional nuisances compared to sample preparation for LSCM, for example. These should be considered when deciding which LSFM platform is most appropriate for an

imaging application. LSFM imaging also can generate terabytes of data quickly, particularly for *Z* stack imaging over time (4-D imaging). Researchers should be prepared and have a plan in place for storing these data and for analyzing them efficiently (Amat et al., 2015). In addition, many image processing programs have limitations in the data size that can be handled. The image analysis program Fiji (Schindelin et al., 2012) with the *BigData Viewer* plugin (Pietzsch, Saalfeld, Preibisch, & Tomancak, 2015) and the open source program *ClearVolume* (Royer et al., 2015) are two free software programs for visualization of this type of data.

DECONVOLUTION FLUORESCENCE MICROSCOPY (DFM)

DFM is a computational image processing technique that can improve image resolution and contrast (Fig. 2.1.10A and 10B). DFM requires knowledge of the idealized or measured point spread function (PSF) of the microscope and the imaging technique used. The PSF that is produced by the microscope system can be used to measure the achievable resolution and give information regarding aberrations induced by the sample or the optics inherent in the microscope. In fact, the 3-D image stack can be viewed as the sum

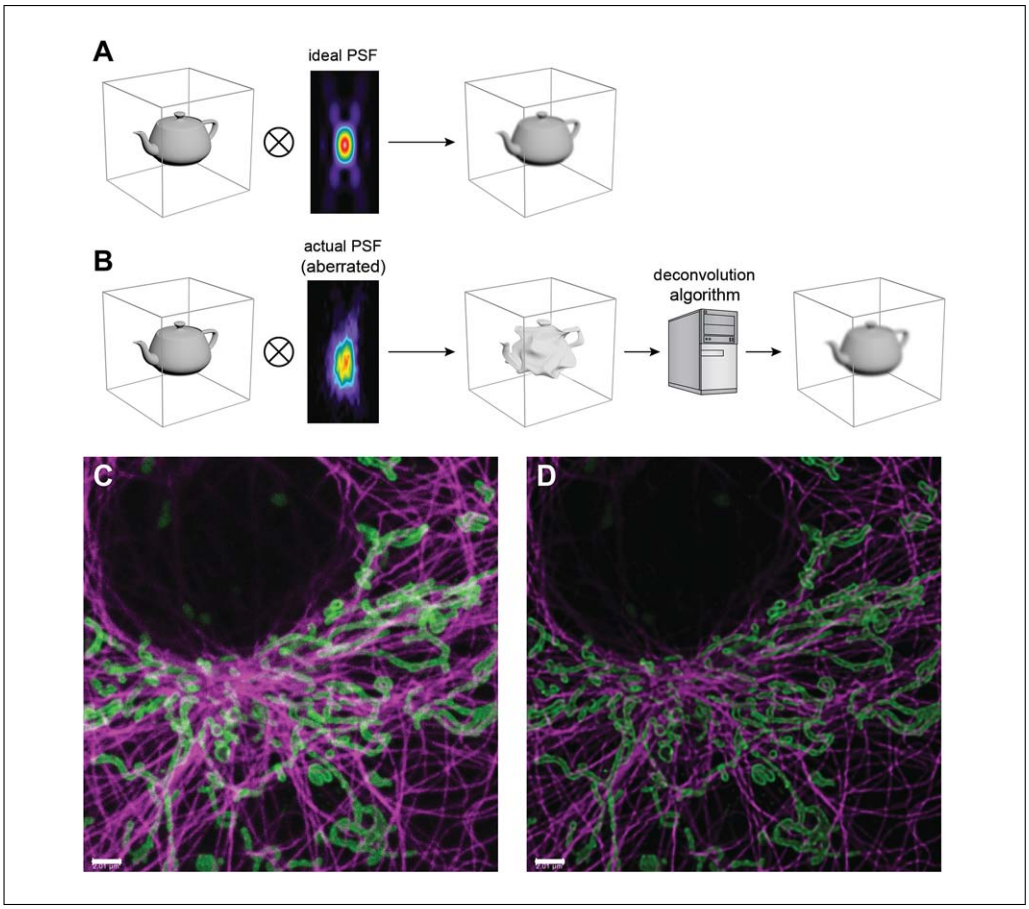

Figure 2.1.10 Deconvolution of fluorescence images. (**A**) Schematic of the deconvolution process. (A) Images produced by microscopes arise from convolution of the microscope's point spread function (PSF) with the image of the real object. The PSF is the 3-D pattern produced by an object that is well below the resolution capability of the instrument, such as a sub-diffractive bead. Even an idealized PSF (shown as a *YZ* orthogonal section) will result in significant loss in resolution and SNR compared to the original object. (**B**) The convolution of the real image with an aberrated PSF results in even more distortion and SNR decrease of the resulting image, which can be corrected with deconvolution. An aberrant PSF can result from distortions induced by the microscope or the sample. Deconvolution seeks to remove these distortions by iteratively restoring light to its proper position in the 3-D image using a model of the PSF. (**C**) Raw maximum intensity (MIP) confocal image of COS7 cells labeled with anti-tubulin and secondary-Alexa 594 (magenta) and mitochondria- anti- Tom 20-secondary with STAR 635P (green) (Abberior). (**D**) Deconvolved image from (B). The deconvolution was done using the Hyugens software program (SVI, NE). Cell images courtesy of Daniela Malide (NHLBI, NIH). Scale bars 2μm in (C) and (D).

of an array of PSFs positioned in space and scaled in intensity. Therefore, the image stack can also be viewed as a convolution between the true data and the PSF of the microscope. The process of reversing this convolution to reduce the effect of aberrations and partially remove the blurring effect of the PSF is thus referred to as deconvolution (Fig. 2.1.10). In practice, the 3-D data and a priori knowledge of the estimated or measured PSF are used by software algorithms to create a new de-blurred 3-D volume image with improved SNR and resolution. This process is usually iterative with the software running the data through a model many times until mathematical errors are minimized or reach a point where further iterations produce no changes in the data. DFM can be used on top of all of the optical techniques mentioned in this review, as long as the PSF is known or can be estimated based on the optics and technique used. Software for image deconvolution is available commercially or through plug-ins for the free image analysis program ImageJ (*http://rsbweb.nih.gov/ij/*, NIH). Although DFM is a powerful technique when used in capable hands (reviews include Boccacci & Bertero, 2002; Biggs, 2010; Helmchen & Denk, 2005; Wallace, Schaefer, & Swedlow, 2001;), the novice user should be warned that deconvolution with incorrect model assumptions can degrade images and/or produce artifacts particularly with images with intrinsically low SNR.

POTENTIAL FUTURE DIRECTIONS

The field of fluorescence microscopy is changing rapidly, as seen by the explosion and subsequent commercialization of new microscopy techniques over the past ten years. One of the biggest concerns moving forward is the massive amount of data that can be acquired with many types of experiments. Storing and analyzing these data can be a challenge. It is likely that there will be an increasing emphasis on "Smart Microscopes" (Scherf & Huisken, 2015) that employ sophisticated software and hardware control to aid the user in obtaining measurements in real time—both with an eye to reducing the overall data volume and to tailoring the acquisition for the specific sample under study. It is also expected that probes will continue to improve—yielding dyes that are smaller, brighter, more photostable, with more and better targeting options, and in more colors than today's palette. The recent development of the silicon-rhodamine (SiR) dyes (Lukinavicius et al., 2013) and their rapid incorporation into the super-resolution imaging field emphasize this point. Recent reviews on the latest in probe technology, including optical sensors, and two-photon and super-resolution probes are a good starting point for what is available now and what is on the horizon (Bolbat & Schultz, 2016; Dempsey, Vaughan, Chen, Bates, & Zhuang, 2011; Mütze et al., 2012; Pak, Swamy, & Yoon, 2015; Ni, Zhuo, So, & Yu, 2016a).

Another important area where we can expect improvement is the preservation of image quality at increasing distances from the coverslip. While it is true that two-photon excitation wavelengths penetrate deeper into tissue, it is still difficult to maintain an aberration-free wave-front (resulting in a diffraction-limited PSF) deep in tissue. Adaptive optics (wavefront measurement and subsequent correction) in its many implementations (Debarre, Botcherby, Booth, & Wilson, 2008; Gould, Burke, Bewersdorf, & Booth, 2012; Ji, Milkie, & Betzig, 2010; Rueckel, Mack-Bucher, & Denk, 2006) show promise but are expensive, difficult to implement, and have yet to see widespread integration and turn-key adoption in commercial microscopes. Along with adaptive optics, it is likely that deconvolution algorithms will improve with better understanding of how the PSF varies spatially in the sample. Both developments will result in higher resolution images with better SNR in thick samples, if implemented correctly.

While we expect images will become ever easier to obtain, "picking the right tool for the job" remains essential. Educating ourselves as to the relative strengths, physical principles, and limitations of each technique is of critical importance, as the alternative— incorrect, misinterpreted, incomplete, or biased data (Pearson, 2007)—remains a risk.

ACKNOWLEDGMENTS

The authors thank Ethan Taylor and Alan Hoofring of the NIH Medical Arts division for help with many of the figures in this work, Dr. Jay Knutson for many helpful discussions and Dr. Henry Eden for proof reading this manuscript. The authors also thank those who permitted reprinting of some of the figures in this article. This work was supported by the intramural research programs of the National Heart Lung and Blood Institute, NIH and the National Institute of Biomedical Imaging and Bioengineering, NIH. The mention of

any company, product, or service in this work is in no way intended as an endorsement by the National Institutes of Health or the authors.

LITERATURE CITED

Amat, F., Hockendorf, B., Wan, Y., Lemon, W. C., McDole, K., & Keller, P. J. (2015). Efficient processing and analysis of large-scale light-sheet microscopy data. *Nature Protocols*, *10*, 1679–1696. doi: 10.1038/nprot.2015.111.

Betzig, E., Patterson, G. H., Sougrat, R., Lindwasser, O. W., Olenych, S., Bonifacino, J. S., ... Hess, H. F. (2006). Imaging intracellular fluorescent proteins at nanometer resolution. *Science*, *313*, 1642–1645.

Biggs, D. S. (2010). 3D deconvolution microscopy. *Current Protocols in Cytometry*, *52*, 12.19.1–12.19.20. doi: 10.1002/0471142956.cy1219s52.

Boccacci, P., & Bertero, M. (2002). Image-restoration methods: Basics and algorithms. In: A. Diaspro, (Ed.), *Confocal and two-photon Mmcroscopy: Foundations, applications, and advances* (pp. 253–269). New York: Wiley-Liss.

Bolbat, A., & Schultz, C. (2016). Recent developments of genetically encoded optical sensors for cell biology. *Molecular Biology of the Cell*. doi: 10.1111/boc.201600040.

Campagnola, P. J., & Loew, L. M. (2003). Second-harmonic imaging microscopy for visualizing biomolecular arrays in cells, tissues and organisms. *Nature Biotechnology*, *21*, 1356–1360. doi: 10.1038/nbt894.

Chen, B. C., Legant, W. R., Wang, K., Shao, L., Milkie, D. E., Davidson, M. W., ... Betzig, E. (2014). Lattice light-sheet microscopy: Imaging molecules to embryos at high spatiotemporal resolution. *Science*, *346*, 1257998. doi: 10.1126/science.1257998.

Coling, D., & Kachar, B. (2001). Theory and application of fluorescence microscopy. *Current Protocols in Neuroscience*, *00*, 2.1.1–2.1.11. doi: 10.1002/0471142301.ns0201s00.

Cox, S., & Jones, G. E. (2013). Imaging cells at the nanoscale. *The International Journal of Biochemistry & Cell Biology*, *45*, 1669–1678. doi: 10.1016/j.biocel.2013.05.010.

Debarre, D., Botcherby, E. J., Booth, M. J., & Wilson, T. (2008). Adaptive optics for structured illumination microscopy. *Opt Express*, *16*, 9290–9305. doi: 10.1364/OE.16.009290.

Dempsey, G. T., Vaughan, J. C., Chen, K. H., Bates, M., & Zhuang, X. (2011). Evaluation of fluorophores for optimal performance in localization-based super-resolution imaging. *Nature Methods*, *8*, 1027–1036. doi: 10.1038/nmeth.1768.

Denk, W., Strickler, J., & Webb, W. (1990). Two-photon laser scanning fluorescence microscopy. *Science*, *248*, 73–76. doi: 10.1126/science.2321027.

Diaspro, A., Bianchini, P., Vicidomini, G., Faretta, M., Ramoino, P., & Usai, C. (2006). Multi-photon excitation microscopy. *Biomedical Engineering Online*, *5*, 36. doi: 10.1186/1475-925X-5-36.

Dickinson, M. E., Bearman, G., Tille, S., Lansford, R., & Fraser, S. E. (2001). Multi-spectral imaging and linear unmixing add a whole new dimension to laser scanning fluorescence microscopy. *Biotechniques*, *31*, 1272, 1274–1276, 1278.

Drobizhev, M., Makarov, N. S., Tillo, S. E., Hughes, T. E., & Rebane, A. (2011). Two-photon absorption properties of fluorescent proteins. *Nature Methods*, *8*, 393–399. doi: 10.1038/nmeth.1596.

Egner, A., Andresen, V., & Hell, S. W. (2002). Comparison of the axial resolution of practical Nipkow-disk confocal fluorescence microscopy with that of multifocal multiphoton microscopy: Theory and experiment. *Journal of Microscopy*, *206*, 24–32. doi: 10.1046/j.1365-2818.2002.01001.x.

Folling, J., Bossi, M., Bock, H., Medda, R., Wurm, C. A., Hein, B., ... Hell, S. W. (2008). Fluorescence nanoscopy by ground-state depletion and single-molecule return. *Nature Methods*, *5*, 943–945.

Gould, T. J., Burke, D., Bewersdorf, J., & Booth, M. J. (2012). Adaptive optics enables 3D STED microscopy in aberrating specimens. *Optics Express*, *20*, 20998–21009. doi: 10.1364/OE.20.020998.

Gustafsson, M. G. (2000). Surpassing the lateral resolution limit by a factor of two using structured illumination microscopy. *Journal de Microscopie*, *198*, 82–87. doi: 10.1046/j.1365-2818.2000.00710.x.

Han, R., Li, Z., Fan, Y., & Jiang, Y. (2013). Recent advances in super-resolution fluorescence imaging and its applications in biology. *Journal of Genetics and Genomics = Yi Chuan Xue Bao*, *40*, 583–595. doi: 10.1016/j.jgg.2013.11.003.

Helmchen, F., & Denk, W. (2005). Deep tissue two-photon microscopy. *Nature Methods*, *2*, 932–940. doi: 10.1038/nmeth818.

Henriques, R., Lelek, M., Fornasiero, E. F., Valtorta, F., Zimmer, C., & Mhlanga, M. M. (2010). QuickPALM: 3D real-time photoactivation nanoscopy image processing in Image. *Journal Nature Methods*, *7*, 339–340. doi: 10.1038/nmeth0510-339.

Hess, S. T., Girirajan, T. P., & Mason, M. D. (2006). Ultra-high resolution imaging by fluorescence photoactivation localization microscopy. *Biophysical Journal*, *91*, 4258–4272.

Hibbs, A. R. (2004). *Confocal microscopy for biologists*. New York, NY: Springer.

Huisken, J., & Stainier, D. Y. (2007). Even fluorescence excitation by multidirectional selective plane illumination microscopy (mSPIM). *Optics Letters*, *32*, 2608–2610. doi: 10.1364/OL.32.002608.

Huisken, J., Swoger, J., Del Bene, F., Wittbrodt, J., & Stelzer, E. H. (2004). Optical sectioning deep inside live embryos by selective plane illumination microscopy. *Science*, *305*, 1007–1009. doi: 10.1126/science.1100035.

Ingaramo, M., York, A. G., Hoogendoorn, E., Postma, M., Shroff, H., & Patterson, G. H. (2014). Richardson-Lucy deconvolution as a general tool for combining images with complementary strengths. *Chemphyschem*, *15*, 794–800. doi: 10.1002/cphc.201300831.

Inoue, S., & Spring, K. R. (1997). *Video microscopy: The fundamentals*. New York, NY: Springer.

Ji, N., Milkie, D. E., & Betzig, E. (2010). Adaptive optics via pupil segmentation for high-resolution imaging in biological tissues. *Nature Methods*, *7*, 141–147. doi: 10.1038/nmeth.1411.

Kaufmann, A., Mickoleit, M., Weber, M., & Huisken, J. (2012). Multilayer mounting enables long- term imaging of zebrafish development in a light sheet microscope. *Development*, *139*, 3242–3247. doi: 10.1242/dev.082586.

Keller, P. J., Schmidt, A. D., Wittbrodt, J., & Stelzer, E. H. (2008). Reconstruction of zebrafish early embryonic development by scanned light sheet microscopy. *Science*, *322*, 1065–1069. doi: 10.1126/science.1162493.

Kellner, R. R., Baier, C. J., Willig, K. I., Hell, S. W., & Barrantes, F. J. (2007). Nanoscale organization of nicotinic acetylcholine receptors revealed by stimulated emission depletion microscopy. *Neuroscience*, *144*, 135–143. doi: 10.1016/j.neuroscience.2006.08.071.

Kobat, D., Durst, M. E., Nishimura, N., Wong, A. W., Schaffer, C. B., & Xu, C. (2009). Deep tissue multiphoton microscopy using longer wavelength excitation. *Optics Express*, *17*, 13354–13364. doi: 10.1364/OE.17.013354.

Kumar, A., Wu, Y., Christensen, R., Chandris, P., Gandler, W., McCreedy, E., ... Shroff, H. (2014). Dual-view plane illumination microscopy for rapid and spatially isotropic imaging. *Nature Protocols*, *9*, 2555–2573. doi: 10.1038/nprot.2014.172.

Lichtman, J. W., & Conchello, J. A. (2005). Fluorescence microscopy. *Nature Methods*, *2*, 910–919. doi: 10.1038/nmeth817.

Livet, J., Weissman, T. A., Kang, H., Draft, R. W., Lu, J., Bennis, R. A., ... Lichtman, J. W. (2007). Transgenic strategies for combinatorial expression of fluorescent proteins in the nervous system. *Nature*, *450*, 56–62. doi: 10.1038/nature06293.

Lukinavicius, G., Umezawa, K., Olivier, N., Honigmann, A., Yang, G., Plass, T., ... Johnsson, K. (2013). A near-infrared fluorophore for live-cell super-resolution microscopy of cellular proteins. *Nature Chemical Biology*, *5*, 132–139. doi: 10.1038/nchem.1546.

Mostany, R., Miquelajauregui, A., Shtrahman, M., & Portera-Cailliau, C. (2015). Two-photon excitation microscopy and its applications in neuroscience. In: J. P. Verveer, (Ed.), *Advanced fluorescence microscopy: Methods and protocols* (pp. 25–42). New York, NY: Springer New York.

Mütze, J., Iyer, V., Macklin, J. J., Colonell, J., Karsh, B., Petrášek, Z., ... Harris, T. D. (2012). Excitation spectra and brightness optimization of two-photon excited probes. *Biophysical Journal*, *102*, 934–944. doi: 10.1016/j.bpj.2011.12.056.

Neil, M. A., Squire, A., Juskaitis, R., Bastiaens, P. I., & Wilson, T. (2000). Wide-field optically sectioning fluorescence microscopy with laser illumination. *Journal de Microscopie*, *197*, 1–4. doi: 10.1046/j.1365-2818.2000.00656.x.

Ni, M., Zhuo, S., So, P. T., & Yu, H. (2016a). Fluorescent probes for nanoscopy: Four categories and multiple possibilities. *Journal of Biophotonics.* doi: 10.1002/jbio.201600042.

Ni, M., Zhuo, S., So, P. T. C., & Yu, H. (2016b). Fluorescent probes for nanoscopy: Four categories and multiple possibilities. *Journal of Biophotonics*, n/a-n/a.

Pak, Y. L., Swamy, K. M., & Yoon, J. (2015). Recent progress in fluorescent imaging probes. *Sensors (Basel)*, *15*, 24374–24396. doi: 10.3390/s150924374.

Patterson, G., Davidson, M., Manley, S., & Lippincott-Schwartz, J. (2010). Superresolution imaging using single-molecule localization. *Annual Review of Physical Chemistry*, *61*, 345–367. doi: 10.1146/annurev.physchem.012809.103444.

Pawley, J. B. (Ed.) (2006). Handbook of biological confocal microscopy. New York, NY: Springer.

Pearson, H. (2007). The good, the bad and the ugly. *Nature*, *447*, 138–140. doi: 10.1038/447138a.

Pellett, P. A., Sun, X., Gould, T. J., Rothman, J. E., Xu, M. Q., Correa, I. R., Jr., & Bewersdorf, J. (2011). Two-color STED microscopy in living cells. *Biomedical Optics Express*, *2*, 2364–2371. doi: 10.1364/BOE.2.002364.

Pietzsch, T., Saalfeld, S., Preibisch, S., & Tomancak, P. (2015). BigDataViewer: Visualization and processing for large image data sets. *Nature Methods*, *12*, 481–483. doi: 10.1038/nmeth.3392.

Royer, L. A., Weigert, M., Gunther, U., Maghelli, N., Jug, F., Sbalzarini, I. F., & Myers, E. W. (2015). ClearVolume: Open-source live 3D visualization for light-sheet microscopy. *Nature methods*, *12*, 480–481. doi: 10.1038/nmeth.3372.

Rueckel, M., Mack-Bucher, J. A., & Denk, W. (2006). Adaptive wavefront correction in two-photon microscopy using coherence-gated wavefront sensing. *Proceedings of the National Academy of Sciences of the United States of America*, *103*, 17137–17142. doi: 10.1073/pnas.0604791103.

Rust, M. J., Bates, M., & Zhuang, X. (2006). Sub-diffraction-limit imaging by stochastic optical reconstruction microscopy (STORM). *Nature Methods*, *3*, 793–795.

Scherf, N., & Huisken, J. (2015). The smart and gentle microscope. *Nature Biotechnology*, *33*, 815–818. doi: 10.1038/nbt.3310.

Schermelleh, L., Carlton, P. M., Haase, S., Shao, L., Winoto, L., Kner, P., ... Sedat, J. W. (2008). Subdiffraction multicolor imaging of the

nuclear periphery with 3D structured illumination microscopy. *Science*, *320*, 1332–1336. doi: 10.1126/science.1156947.

Schindelin, J., Arganda-Carreras, I., Frise, E., Kaynig, V., Longair, M., Pietzsch, T., ... Cardona, A. (2012). Fiji: An open-source platform for biological-image analysis. *Nature Methods*, *9*, 676–682. doi: 10.1038/nmeth.2019.

Schmidt, R., Wurm, C. A., Jakobs, S., Engelhardt, J., Egner, A., & Hell, S. W. (2008). Spherical nanosized focal spot unravels the interior of cells. *Nature Methods*, *5*, 539–544. doi: 10.1038/nmeth.1214.

Shaner, N. C., Steinbach, P. A., & Tsien, R. Y. (2005). A guide to choosing fluorescent proteins. *Nature Methods*, *2*, 905–909. doi: 10.1038/nmeth819.

Sharonov, A., & Hochstrasser, R. M. (2006). Wide-field subdiffraction imaging by accumulated binding of diffusing probes. *Proceedings of the National Academy of Sciences of the United States of America*, *103*, 18911–18916. doi: 10.1073/pnas.0609643104.

Spiess, E., Bestvater, F., Heckel-Pompey, A., Toth, K., Hacker, M., Stobrawa, G., ... Acker, H. (2005). Two-photon excitation and emission spectra of the green fluorescent protein variants ECFP, EGFP and EYFP. *Journal of Microscopy*, *217*, 200–204. doi: 10.1111/j.1365-2818.2005.01437.x.

Svoboda, K., & Yasuda, R. (2006). Principles of two-photon excitation microscopy and its applications to neuroscience. *Neuron*, *50*, 823–839. doi: 10.1016/j.neuron.2006.05.019.

Thompson, R. E., Larson, D. R., & Webb, W. W. (2002). Precise nanometer localization analysis for individual fluorescent probes. *Biophysical Journal*, *82*, 2775–2783. doi: 10.1016/S0006-3495(02)75618-X.

Toomre, D., & Bewersdorf, J. (2010). A new wave of cellular imaging. *Annual Review of Cell and Developmental Biology*, *26*, 285–314. doi: 10.1146/annurev-cellbio-100109-104048.

Toomre, D., & Manstein, D. J. (2001). Lighting up the cell surface with evanescent wave microscopy. *Trends in Cell Biology*, *11*, 298–303. doi: 10.1016/S0962-8924(01)02027-X.

Uno, S.-n., Tiwari, D. K., Kamiya, M., Arai, Y., Nagai, T., & Urano, Y. (2015). A guide to use photocontrollable fluorescent proteins and synthetic smart fluorophores for nanoscopy. *Microscopy*, *64*, 263–277. doi: 10.1093/jmicro/dfv037.

Urban, N. T., Willig, K. I., Hell, S. W., & Nagerl, U. V. (2011). STED nanoscopy of actin dynamics in synapses deep inside living brain slices. *Biophysical Journal*, *101*, 1277–1284. doi: 10.1016/j.bpj.2011.07.027.

Vadakkan, T. J., Culver, J. C., Gao, L., Anhut, T., & Dickinson, M. E. (2009). Peak multiphoton excitation of mCherry using an optical parametric oscillator (OPO). *Journal of Fluorescence*, *19*, 1103–1109. doi: 10.1007/s10895-009-0510-y.

Vicidomini, G., Schonle, A., Ta, H., Han, K. Y., Moneron, G., Eggeling, C., & Hell, S. W. (2013). STED nanoscopy with time-gated detection: Theoretical and experimental aspects. *PLoS One*, *8*, e54421. doi: 10.1371/journal.pone.0054421.

Wallace, W., Schaefer, L. H., & Swedlow, J. R. (2001). A workingperson's guide to deconvolution in light microscopy. *Biotechniques*, *31*, 1076–1078, 1080, 1082 passim.

Willig, K. I., Harke, B., Medda, R., & Hell, S. W. (2007). STED microscopy with continuous wave beams. *Nature Methods*, *4*, 915–918. doi: 10.1038/nmeth1108.

Willig, K. I., Rizzoli, S. O., Westphal, V., Jahn, R., & Hell, S. W. (2006). STED microscopy reveals that synaptotagmin remains clustered after synaptic vesicle exocytosis. *Nature*, *440*, 935–939. doi: 10.1038/nature04592.

Winter, P. W., Chandris, P., Fischer, R. S., Wu, Y., Waterman, C. M., & Shroff, H. (2015). Incoherent structured illumination improves optical sectioning and contrast in multiphoton super-resolution microscopy. *Optics Express*, *23*, 5327–5334. doi: 10.1364/OE.23.005327.

Winter, P. W., York, A. G., Nogare, D. D., Ingaramo, M., Christensen, R., Chitnis, A., ... Shroff, H. (2014). Two-photon instant structured illumination microscopy improves the depth penetration of super-resolution imaging in thick scattering samples. *Optica*, *1*, 181–191. doi: 10.1364/OPTICA.1.000181.

Wu, Y., Ghitani, A., Christensen, R., Santella, A., Du, Z., Rondeau, G., ... Shroff, H. (2011). Inverted selective plane illumination microscopy (iSPIM) enables coupled cell identity lineaging and neurodevelopmental imaging in Caenorhabditis elegans. *Proceedings of the National Academy of Sciences of the United States of America*, *108*, 17708–17713. doi: 10.1073/pnas.1108494108.

Wu, Y., Wawrzusin, P., Senseney, J., Fischer, R. S., Christensen, R., Santella, A., ... Shroff, H. (2013). Spatially isotropic four-dimensional imaging with dual-view plane illumination microscopy. *Nature Biotechnology*, *31*, 1032–1038. doi: 10.1038/nbt.2713.

Wu, Y., Chandris, P., Winter, P. W., Kim, E. Y., Jaumouillé, V., Kumar, A., ... Shroff, H. (2016). Simultaneous multiview capture and fusion improves spatial resolution in wide-field and light-sheet microscopy. *Optica*, *3*, 897–910. doi: 10.1364/OPTICA.3.000897.

York, A. G., Chandris, P., Nogare, D. D., Head, J., Wawrzusin, P., Fischer, R. S., ... Shroff, H. (2013). Instant super-resolution imaging in live cells and embryos via analog image processing. *Nature Methods*, *10*, 1122–1126. doi: 10.1038/nmeth.2687.